

IG²: Integrated Gradient on Iterative Gradient Path for Feature Attribution

Yue Zhuo, Zhiqiang Ge, *Senior Member, IEEE*

Abstract—Feature attribution explains Artificial Intelligence (AI) at the instance level by providing importance scores of input features' contributions to model prediction. Integrated Gradients (IG) is a prominent path attribution method for deep neural networks, involving the integration of gradients along a path from the explained input (explicand) to a counterfactual instance (baseline). Current IG variants primarily focus on the gradient of explicand's output. However, our research indicates that the gradient of the counterfactual output significantly affects feature attribution as well. To achieve this, we propose Iterative Gradient path Integrated Gradients (IG²), considering both gradients. IG² incorporates the counterfactual gradient iteratively into the integration path, generating a novel path (*GradPath*) and a novel baseline (*GradCF*). These two novel IG components effectively address the issues of attribution noise and arbitrary baseline choice in earlier IG methods. IG², as a path method, satisfies many desirable axioms, which are theoretically justified in the paper. Experimental results on XAI benchmark, ImageNet, MNIST, TREC questions answering, wafer-map failure patterns, and CelebA face attributes validate that IG² delivers superior feature attributions compared to the state-of-the-art techniques. The code is released at: <https://github.com/JoeZhuo-ZY/IG2>.

Index Terms—Feature Attribution, Integrated Gradient, eXplainable Artificial Intelligence (XAI), Counterfactual Explanation

1 INTRODUCTION

AI models are becoming increasingly prevalent in critical fields, such as industrial control and biomedical analysis. Consequently, the need for research into their explainability (XAI) has become urgent. This is essential to keep humans in the loop and help people understand, explain, and control the models [1], [2], [3]. Given an input instance (e.g., an image), feature attribution for deep neural networks quantifies the contributions of individual features, such as pixels, to the model output. These results can support the users in reasoning which input elements drive model predictions.

The gradient is a basic form of feature attribution that analogizes the model's coefficients for a deep network. Early local gradient methods such as Vanilla Gradient [4], Grad-CAM [5], and Guided Backpropagation [6] suffer from the gradient saturation, a problem that the gradients in the input neighborhood are misleading [7], [8]. Recently, for solving this problem, Integrated Gradients (IG) [9] was proposed as a path method that integrates gradient (of model output) along a path between the explained instance (i.e., explicand) and baseline.

IG methods introduce the concept of counterfactual explanation, which contrastively explain the models by answering: "Which features cause the model output prediction A (of explicand) rather than counterfactual prediction B

(of baseline)?" From the perspectives of philosophy and psychology, the counterfactuals align with human cognition to explain unexpected events [10], [11], and have been implied in many attribution methods, such as SHapley Additive exPlanations [12], DeepLIFT [7], SCOUT [13], and sub-region interpretation [14].

The focus of this study is on IG, a well-known path (attribution) method for deep neural networks. Path methods, rooted in Aumann-Shapley game theory, adhere to many describable axioms [17], [9]. IG's attribution performance depends on two essential hyperparameters: path and baseline. The conventional approach, Vanilla IG, typically employs a zero baseline (e.g., all-black image) along with a straight-line path. However, this choice is arbitrary and agnostic to the model and explicand, leading to several shortcomings. For instance, the straight-line path can introduce noise into the attribution due to the saturation effect [18] and the use of a black baseline will result in incomplete attributions [19], [20].

Recently, with different paths and baselines, many variant path methods have been proposed for improving attributions. For integration paths, Guided IG [23] adaptively chooses the path by selecting features with the smallest partial derivatives; Blur IG [24] integrated the gradients on the gradually blurred image path. For baselines, Expected IG [19] sampled the baselines from the data distribution; Sturmfels et al. [20] discussed different baselines' impacts on the path methods.

Notably, despite these advancements, the majority of existing baselines and paths are considered model-agnostic and explicand-agnostic. We believe the excellent baseline

1. Note that the terms *counterfactuals* [11], *contrastive facts* [15], and *counter (class) example* [16] are used interchangeably in prior explanation works. In the context of Shapley value [12] and path methods [9], they are commonly referred to as *background* and *baseline*.

- This paper has been accepted by *IEEE Transactions on Pattern Analysis and Machine Intelligence*.
- This work was supported in part by the National Natural Science Foundation of China (NSFC) (92167106, 62103362 and 61833014) and the Natural Science Foundation of Zhejiang Province (LR18F030001). (Corresponding author: Zhiqiang Ge)
- Yue Zhuo is with the State Key Laboratory of Industrial Control Technology, College of Control Science and Engineering, Zhejiang University, Hangzhou, 310027, China. Zhiqiang Ge is with Peng Cheng Laboratory, Shenzhen, 518000, China. (E-mail: zhuoy1995@zju.edu.cn, zhiqiang.ge@hotmail.com)

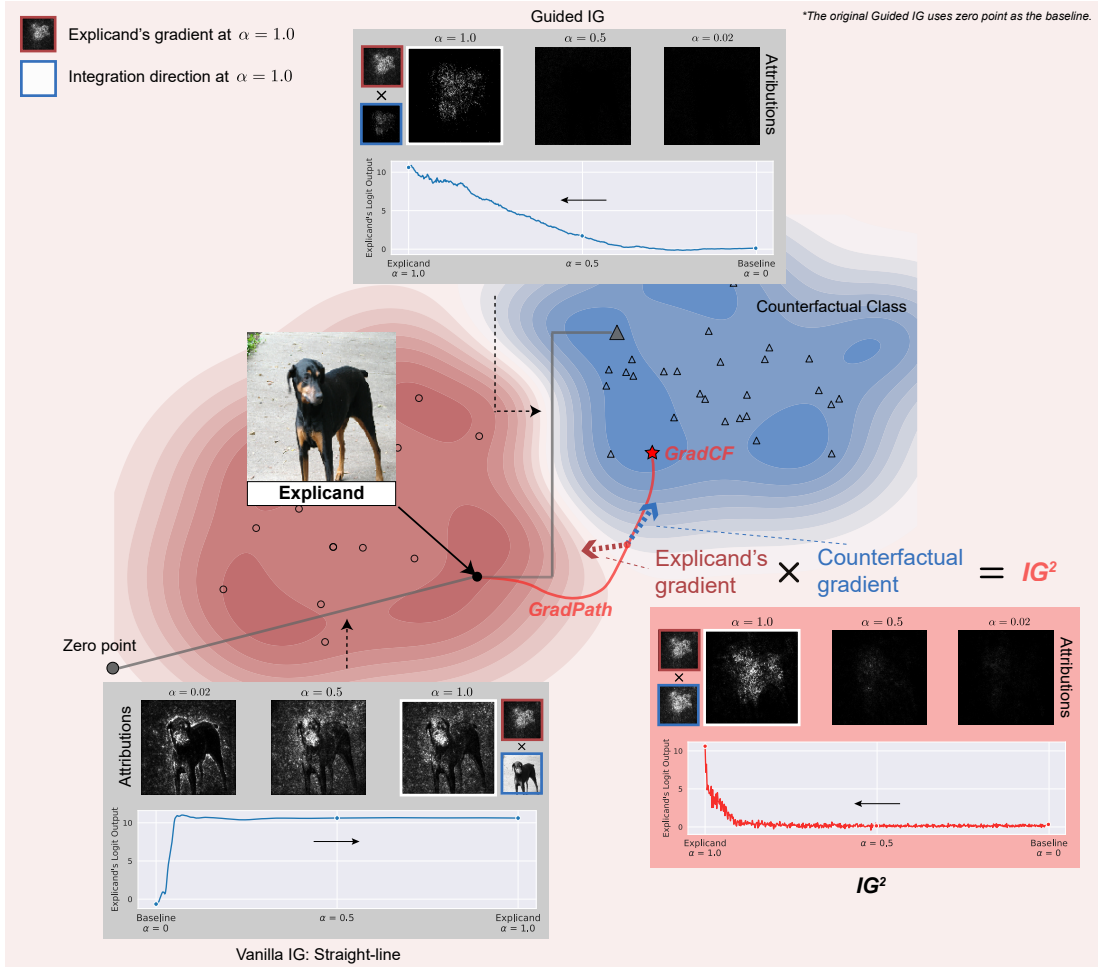


Fig. 1: **Illustration of IG^2 with GradPath and GradCF**, compared with Vanilla IG (with a zero baseline) and Guided IG (counterfactual baseline). The explicand is a sample [Doberman] from ImageNet [21] classified by Inception-v3 [22]. The graphs of logit predictions for [Doberman] w.r.t. α value are plotted. The attributions snapshots of each method are shown at α values of 0.02, 0.5 and 1.0. At $\alpha = 1.0$, the attributions are decomposed into two multipliers: explicand’s gradient (small images in red boxes) and integration path direction (in blue boxes). Integration path of IG^2 optimally aligns the explicand’s gradient with the counterfactual gradient. This alignment results in feature attributions that are less noisy and more complete (on the body of Doberman). Comprehensive attribution results on ImageNet can be found in Section 6.3.

and path should contain the information of both explicand and model, which motivates the idea of IG^2 . Table 1 summarizes the existing IG-based methods from paths and baselines, and Section 5.2 contrasts them with our proposal in detail.

IG^2 : Fig. 1 depicts IG^2 . Starting from the explicand, IG^2 iteratively searches the instances in the descent direction of the counterfactual gradient, minimizing the representation distance between the explicand and counterfactual. The set of all samples searched at each step is denoted as GradPath, and its endpoint is the baseline GradCF, a counterfactual (CF) example. As the name suggests, IG^2 multiplies two gradients during the integration: one of explicand’s prediction and another of the counterfactual class, the latter of which is implied in the GradPath. IG^2 provides superior attributions over existing techniques, due to the distinctions on two essentials of path methods: the integration path and baseline.

GradPath in IG^2 effectively mitigates saturation effects [23], [18] (in Definition 3). This is achieved by its

alignment with the counterfactual gradients, leading to a rapid decrease in the model’s prediction of the explicand. Fig. 1 show the merit of GradPath by the attributions at $\alpha = 1$, where three path share an identical explicand’s gradient. The GradPath, by directing itself towards the salient features that distinguish the explicand and counterfactual, which “filters” the noise in explicand’s gradient by path integration. In contrast, the straight-line in Vanilla IG is on the dissimilar direction to the explicand’s gradient, causing the noise in image background to accumulate along the integration path, leading to saturation effects; Guided IG shares a similar idea with IG^2 but its path direction is constrained, which results in less complete attributions than IG^2 .

GradCF is a novel baseline proposed in IG^2 , and its advantages are illustrated in Fig. 2, contrasting the explicand with different baselines. GradCF can significantly highlight with critical features. For [Doberman] example, GradCF accurately highlights the dog’s body with the counterfactual gradients. On the contrary, using a black baseline disre-

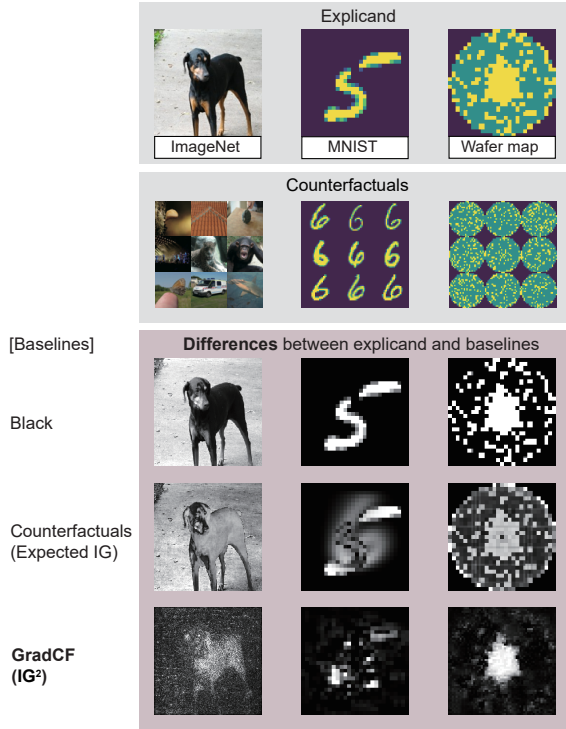


Fig. 2: **Differences between explicand and three baselines:** the black image, counterfactuals and GradCF. Three samples from ImageNet, MNIST [25] and wafer map [25] datasets are plotted. For the non-black baselines of counter class, the ImageNet sample is contrasted with randomly sampled images, MNIST’s digital 5 is contrasted with digitals 6, and the central failure wafer map is contrasted with normal wafer maps. The critical features in explicands are accurately highlighted by contrasting with GradCF. Detailed discussions of GradCF on MNIST examples are in Section 4.2.

gards the black pixels on dog and adversely attributes to the white background instead. While Expected IG employs counterfactual data as the baseline to address this issue, but this naive contrast in the input space remains irrelevant to the explicand, resulting in noises [20]. For other two datasets, GradCF also precisely highlights the key features, distinguishing between digital 5 and digital 6, as well as the defective wafer map in contrast to normal ones.

In this study, our primary contribution is the introduction of IG^2 , a novel path attribution method. IG^2 comprises both a novel baseline, GradCF, and a novel integration path, GradPath. To the best of our knowledge, it is the first time that counterfactual gradients are integrated into the path attribution methods. Through extensive experiments on datasets from diverse domains, both qualitative and quantitative results consistently demonstrate IG^2 ’s superiority over existing state-of-the-art attribution methods. Furthermore, we substantiate the individual effectiveness of GradCF and GradPath through an ablation study.

The remainder of the paper is organized as: Section 2 introduces the preliminary about path methods; Section 3 demonstrates our proposal in detail; Section 4 gives a deep insight into IG^2 and theoretically justify its axioms; Section 5 contrasts our method with related works across different

TABLE 1: Summary of existing path methods from the aspects of path and baseline

Methods	Path	M-s [†] Baseline	E-s [§] M-s [†]
[20]*	straight line	maximal distance noised data uniform noise	✓ ✓
Vanilla IG [9]	straight line	zero vector	
Expected IG [19]	straight line	train data	
XRAI [26]	straight line	black+white images	
Blur IG [24]	blur path	blurred image	✓
Guided IG [23]	straight line’s projection	✓ zero vector	
IG^2 (ours)	GradPath	✓ GradCF	✓ ✓

* Work [20] discussed all the other baselines in Vanilla IG, Expected IG, XRAI, Blur IG, and Guided IG (except ours), which is not listed for clarity.

† M-s (Model-specific): The path (or baseline) is specifically designed for explained models.

§ E-s (Explicand-specific): The baseline is specifically designed for explained sample.

fields; Section 6 presents experimental results to verify the attribution performances of IG^2 ; Section 7 presents the IG^2 implementation details; Section 8 concludes the paper.

2 PRELIMINARY OF PATH METHODS

Path methods are based on the Aumann-Shapley theory from cost-sharing with many desirable properties. Given input instances of n dimension $x \in \mathbb{R}^n$, the path of gradient integral is formally defined as $\gamma(\alpha)$ for $\alpha \in [0, 1]$. Path $\gamma(\alpha) : [0, 1] \rightarrow \mathbb{R}^n$ consists of a set of points in \mathbb{R}^n , from the baseline x' to the explicand x (i.e., $\gamma(0) = x'$ and $\gamma(1) = x$).

Given a path γ and model $f : \mathbb{R}^n \rightarrow \mathbb{R}$ (in classification models, only considering the output of explicand’s class label), path integrated gradient attributes the i^{th} feature by integrating the gradients of the model output w.r.t the i^{th} feature value along the path $\gamma(\alpha)_i$, which is defined as [9]:

$$\phi_i^{Path} = \int_0^1 \frac{\partial f(\gamma(\alpha))}{\partial \gamma(\alpha)_i} \frac{\partial \gamma(\alpha)_i}{\partial \alpha} d\alpha, \quad (1)$$

where the first multiplier is the explicand’s gradient of model prediction and the second one is the path direction.

Baselines: The choices of baseline x' are various, and there is currently no consensus on which baseline is the best. Work [20] carefully researched the mainstream baselines, and we summarized them in Table 1. The zero (black) instance $x' = \vec{0}$, one (white) instance $x' = \vec{1}$ and train data $x' \sim D_{train}$ are three commonly used baselines.

Straight-line path: The commonly used path is the straight line from the explicand x to baseline x' , which is specified $\gamma(\alpha) = x' + \alpha \times (x - x')$ for $\alpha \in [0, 1]$.

In practice, it is intractable to directly compute the integral in Eq. 1. Instead, a Riemann sum is used for a discrete approximate with k points in the integral interval. On a straight-line path, the IG [9] is computed by:

$$\phi_i^{IG} = (x_i - x'_i) \times \sum_{i=1}^k \frac{\partial f(x' + \frac{k}{m} \times (x - x'))}{\partial x_i} \times \frac{1}{m}. \quad (2)$$

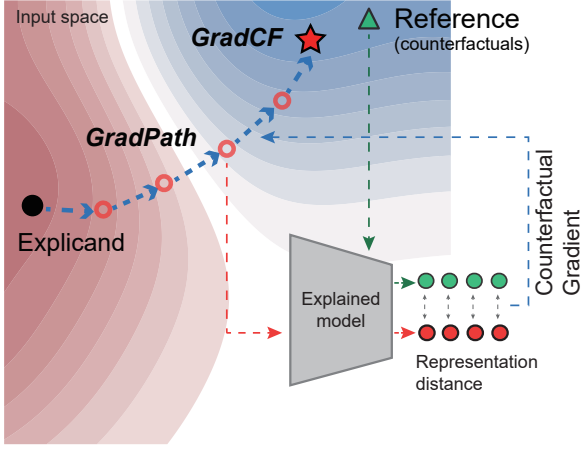


Fig. 3: **Illustration for building GradPath** at each step. From the explicand, the direction of GradPath is iteratively built on the gradient direction for minimizing the model representation distance to the reference.

3 METHODOLOGIES OF IG²

IG² is a path method that extends IG [9] by introducing a novel baseline (GradCF) and a novel integration path (GradPath). As the name suggests, IG² accumulates not only the gradient of the explicand’s prediction but also the counterfactual gradient, the latter of which is contained in the direction of GradPath.

Given an explicand x , IG² first sample a counterfactual reference x^r with the different class label to x . We name x^r reference instead of baseline since it is not the integration endpoint of IG².²

Definition 1. (IG² attribution) Let x^r denote reference, γ^G denote GradPath, f and \tilde{f} denote the prediction and representation layer of the explained model, IG² attribution for the i^{th} feature of explicand x is defined as:

$$\phi_i^{IG^2} = \underbrace{\sum_{j=0}^{k-1} \frac{\partial f(\gamma^G(\frac{j}{k}))}{\partial x_i}}_{\text{explicand's}} \times \underbrace{\frac{\partial \|\tilde{f}(\gamma^G(\frac{j}{k})) - \tilde{f}(x^r)\|_2^2}{\partial x_i}}_{\text{counterfactual}} \times \frac{\eta}{W_j}, \quad (3)$$

where W_j is the normalization coefficient and η is the step size hyperparameter.

Eq. 3 explicitly reveals the nature of IG²: the multiplication of two gradients. Compared to Vanilla IG in Eq. 2, the major distinction is the Riemann summation weight of explicand’s gradients: the weight of counterfactual gradient can highlight the critical features, whereas that in Vanilla IG is a constant. Intuitively, IG² introduces the information of model representation difference rather than naive difference in the input feature space (i.e., $x_i - x_i^r$).

Overall, IG² is built on two stages: building GradPath and integrating gradients on GradPath. The following sections respectively introduce them, deriving IG² in Eq. 3.

2. Counterfactual sample x^r directly serves as the baseline in Expected IG [19].

Algorithm 1 Compute GradPath and GradCF

Input: representation layer: \tilde{f}
 explicand: x
 reference: x^r
 step size: η
 steps: k

- 1: $\delta \leftarrow \vec{0} \triangleleft$ initiate perturbation
- 2: $\gamma^G(1) = x \triangleleft$ initiate GradPath³
- 3: **for** $j = k - 1$ to 0 **do**
- 4: $g = \frac{\partial \|\tilde{f}(x+\delta) - \tilde{f}(x^r)\|_2}{\partial x}$
- 5: $W = \|g\|_{1 \text{ or } 2} \triangleleft \ell_1$ or ℓ_2 norm
- 6: $g = \eta \cdot \frac{g}{W} \triangleleft$ normalized iterative gradient
- 7: $\delta = \delta - g \triangleleft$ update total perturbation
- 8: $\gamma^G(j/k) = x + \delta \triangleleft$ store the CF at each step
- 9: **end for**

Output: GradCF: $\gamma^G(0)$, GradPath: γ^G

3.1 Building GradPath

Fig. 3 illustrates how GradPath is built during the iterative search of GradCF. The motivation of GradCF is to provide a counterfactual explanation:

Given limited perturbation resource, perturbing which features on explicand x can make the model consider the perturbed explicand to be most similar to the (counterfactual) reference x^r ?

This similarity can be measured by the distance between two model representations⁴ and the perturbation search can be converted to a minimization problem. Denoting the network representation by \tilde{f} , the perturbation by δ and Euclidean distance measure by $\|\cdot\|_2^2$, the optimization objective for GradCF is:

$$\min_{\delta} \|\tilde{f}(x + \delta) - \tilde{f}(x^r)\|_2^2. \quad (4)$$

We iteratively solve Eq. 4 using gradient descent with normalization at each step. GradPath γ^G is built during the iteration by the trajectory of normalized gradient descent, and the endpoint $x + \delta$ is the target counterfactual baseline, GradCF.

Algorithm 1 provides the pseudo-code for computing GradCF and GradPath. GradPath can be defined as:

Definition 2. (GradPath) Given reference x^r and model representation \tilde{f} , GradPath is defined by a discrete function γ^G , on a feasible set $\{0, \frac{1}{k}, \dots, \frac{k-1}{k}, 1\}$, for $0 \leq j \leq k - 1$, $j \in \mathbb{N}$:

$$\begin{aligned} \gamma^G(\frac{j}{k}) &= \gamma^G(\frac{j+1}{k}) - \frac{\partial \|\tilde{f}(\gamma^G(\frac{j+1}{k})) - \tilde{f}(x^r)\|_2}{\partial \gamma^G(\frac{j+1}{k})} \frac{\eta}{W_j}, \\ \gamma^G(1) &= x, \end{aligned} \quad (5)$$

where W_j is introduced in Line 5, Algorithm 1.

3. GradPath is built on the opposite direction to the conventional path integration. To match path methods, we set GradPath $\gamma^G(j)$ from $j = 1$ to $j = 0$, so that the optimization iteration starts at the point $\gamma^G(1)$ (explicand) and ends at the point $\gamma^G(0)$ (baseline, GradCF).

4. We use activations in the penultimate layer as the representation. The choice of representation layer is discussed in Appendix A.3.

GradCF as explanation (GradCFE) We can utilize the difference between the GradCF and explicand to provide a counterfactual feature attribution:

$$\text{GradCFE} = x - \gamma^G(0). \quad (6)$$

3.2 Integrating gradients on GradPath

IG^2 integrates feature gradients in the same approach as path methods (in Eq. 1). Since the GradPath γ^G is a discrete function, which does not have continuous gradients $\frac{\partial \gamma(\alpha)}{\partial \alpha}$, we can operate finite difference to approximate the path gradient. Both forward difference and backward difference are feasible. According to Eq. 5, the path gradient of GradPath w.r.t $\alpha = \frac{j}{k}$ can be computed by both two differences:

$$\frac{\partial \gamma^G(\frac{j}{k})}{\partial \frac{j}{k}} = \begin{cases} \frac{\gamma^G(\frac{j+1}{k}) - \gamma^G(\frac{j}{k})}{1/k} = k \frac{\partial \|\tilde{f}(\gamma^G(\frac{j+1}{k})) - \tilde{f}(x^r)\|_2}{\partial \gamma^G(\frac{j+1}{k})} \frac{\eta}{W_j} \\ \frac{\gamma^G(\frac{j}{k}) - \gamma^G(\frac{j-1}{k})}{1/k} = k \frac{\partial \|\tilde{f}(\gamma^G(\frac{j}{k})) - \tilde{f}(x^r)\|_2}{\partial \gamma^G(\frac{j}{k})} \frac{\eta}{W_j} \end{cases}, \quad (7)$$

where the first line is the forward difference and the second is the backward difference.

Using the backward difference in Eq. 7 and Riemann sum of Eq. 1, we derive IG^2 attribution (for the i^{th} feature):

$$\begin{aligned} \phi_i^{\text{IG}^2} &= \int_0^1 \frac{\partial f(\gamma^G(\alpha))}{\partial \gamma^G(\alpha)_i} \frac{\partial \gamma^G(\alpha)_i}{\partial \alpha} d\alpha \\ &\approx \sum_{j=0}^{k-1} \frac{\partial f(\gamma^G(\frac{j}{k}))}{\partial \gamma^G(\frac{j}{k})_i} \times \frac{\partial \|\tilde{f}(\gamma^G(\frac{j}{k})) - \tilde{f}(x^r)\|_2}{\partial \gamma^G(\frac{j}{k})_i} \\ &\quad \times \frac{k\eta}{W_j} \times \left(\frac{j+1-j}{k}\right) \\ &= \sum_{j=0}^{k-1} \frac{\partial f(\gamma^G(\frac{j}{k}))}{\partial x_i} \times \frac{\partial \|\tilde{f}(\gamma^G(\frac{j}{k})) - \tilde{f}(x^r)\|_2}{\partial x_i} \times \frac{\eta}{W_j}, \end{aligned} \quad (8)$$

where the two denominators $\partial \gamma^G(\frac{j}{k})_i$ are substituted as ∂x_i , due to $\gamma^G(\frac{j}{k}) = x + \delta$ (Line 8, Algorithm 1).

Practically, the integration direction (from baseline to explicand) is opposite to the GradPath search direction (from explicand to baseline). Thus, backward difference requires the complete GradPath to be computed first, and then the gradient is integrated. If using forward difference, the gradient integral can be computed simultaneously with the GradPath.

For the implementation details of IG^2 , Section 7 comprehensively discusses the hyperparameter impacts on IG^2 attribution, including reference, step size, step number, normalization, and similarity measures. The IG^2 computational cost is also analyzed and compared with other attribution methods.

4 INTERPRETING IG^2

The novel baseline (GradCF) and novel integration path (GradPath) are two major contributions of IG^2 , so we discuss IG^2 by interpreting the superiority of these two components. Specifically, Section 4.2 and Section 4.1 answer the questions: *Why GradCF and GradPath are better baseline and integration path than the existing methods?*

Theoretically, the desirable axioms of IG^2 and GradCFE are justified in Section 4.3.

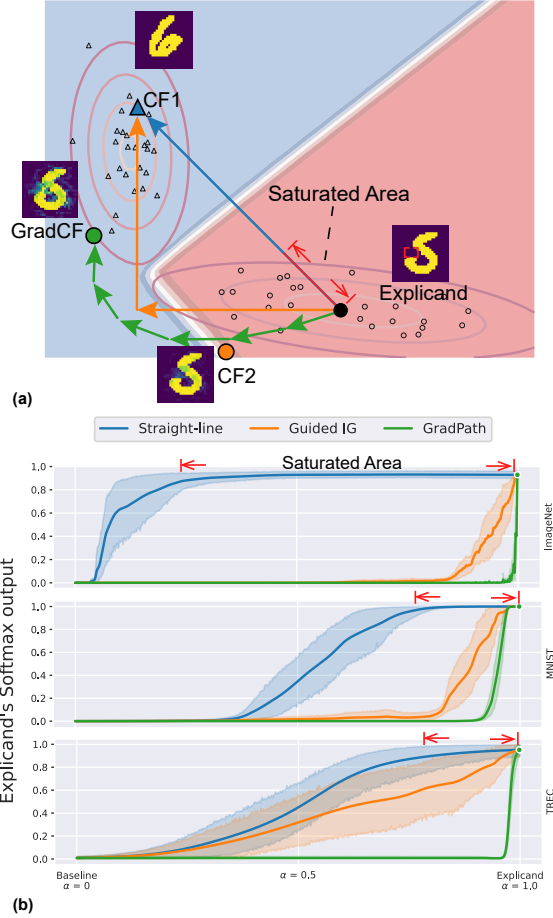


Fig. 4: (a) Illustration for three counterfactual examples and three integration paths: CF1 sampled from counterfactual data distribution, CF2 generated by an adversarial attack and the GradCF using CF1 as the reference. The saturated area on straight-line path is marked in red. An MNIST explicand (digital 5) and three CFs (digital 6) are plotted. **(b) Graphs of explicand's Softmax prediction along integration paths on ImageNet, MNIST, and TREC,** averaged on 100 samples of each dataset.

4.1 GradPath: mitigating saturation effects

The superiority of GradPath for feature attribution is discussed from the perspective of saturation effects.

Definition 3. (Saturation effects) [23], [18] *The straight-line path of IG is susceptible to travel through the saturated area where model output is not changing substantially with respect to α . In this area, the feature gradient is not pointing toward the integration path. This phenomenon leads to the accumulation of noisy attributions, called saturation effects.*

The integral value in Eq. 1 can be decomposed into two multipliers: (input) feature gradient and path direction. The presence of a saturated area indicates that the feature gradient and integration path are in dissimilar directions (otherwise, the model prediction should drop quickly), which means the path is not moving on the important features. This will result in incorrect feature attributions, and a good integration path should avoid this undesirable area.

The saturation effects were analyzed in works [23], [18].

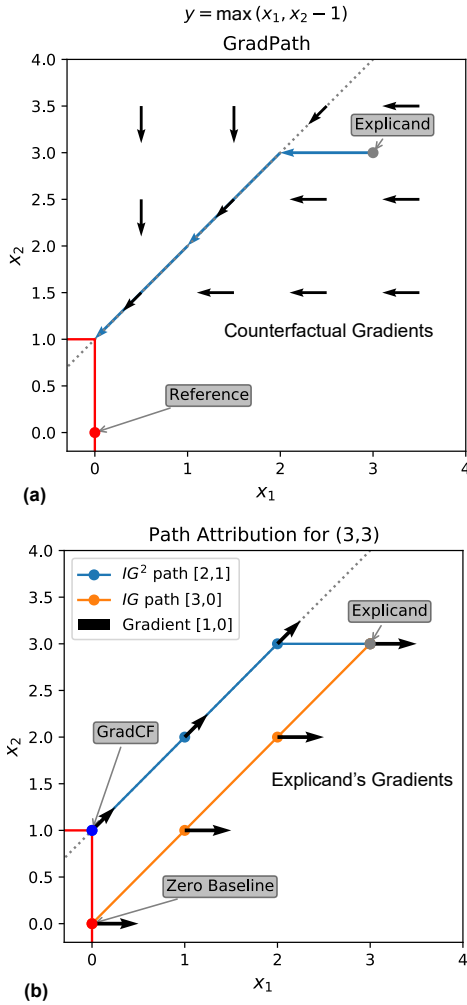


Fig. 5: **The toy example for feature attribution** with function $y = \max(x_1, x_2 - 1)$ on explicand $(x_1, x_2) = (3, 3)$ with the zero reference $(0, 0)$. (a) GradPath on counterfactual gradients in blue line. (b) The attribution results of three methods in the legend.

Some techniques have been proposed for this issue, for example, averaging over multiple straight paths [26], [27] and splitting the straight paths into different segments [18]. Guided IG [23] explicitly avoids the saturated area by designing the path based on the absolute values of feature gradients. However, the path of Guided IG is still constrained in the hyper-rectangular with the straight-line path as diagonal.

GradPath effectively mitigates the saturation effects. Recalling the objective of GradCF in Eq. 4, we minimize the distance to the counterfactual model representation, which implicitly means the explicand's prediction is meanwhile minimized. Each step of GradPath points toward the steep direction that rapidly decreases the model prediction (shown in Fig. 4).

As a supplementary for graphs in Fig. 1, Fig. 4b displays the average output curves on three datasets. Compared with straight line, Guided IG's path and GradPath both avoid the saturated area. Since Guided IG's path is restricted, GradPath can get out of the saturated area more quickly.

Toy example: Fig. 5 displays a toy example, showing GradPath contributes to better feature attribution. Because x_2 is always smaller than x_1 on the straight-line path, the max function signs zero gradients on the smaller feature (right black arrows). This causes IG and gradient methods both assign zero attribution on feature x_2 , which is inconsistent with intuition. Contrarily, integrated gradients on GradPath give nonzero attribution on x_2 with a more reasonable baseline, GradCF $(0, 1)$.

4.2 GradCF

Based on works in the field of counterfactual explanation (CFE), we summarize a good counterfactual baseline in path methods should have the following desirable properties:

- **Validity** [11] The counterfactual baseline should be classified in the desired class (different from the explicand).
- **Data manifold closeness** [28] It would be hard to trust a counterfactual if it resulted in a combination of features that were utterly unlike any observations the classifier has seen before. Therefore, a generated counterfactual should be realistic in the sense that it is near the training data.
- **Explicand relevance** A good counterfactual example should be related to the explicand to directly contrast features. Though almost all the CFE methods [28] generate counterfactual examples based on the explicand, the baselines of most existing path methods are explicand-agnostic (see Table 1).

The commonly used uninformative baselines (black and white) violate all three properties, which are unrealistic and do not have any information on classes. For instance, the black pixel will not be attributed with an all-black baseline, even though it contributes to the model output.

Expected IG [19] solves this by using the samples from the data distribution (CF1 in Fig. 4), which satisfies the validity and data manifold closeness. However, the sampling procedure of train data is *explicand-agnostic*, which provides inaccurate contrast in the feature space (discussed in Fig. 6a).

A basic counterfactual example (CF2 in Fig. 4) is also compared. CF2 is generated with projected gradient descent (PGD) [29] attack for the minimal perturbation that causes the model to give a counterfactual prediction [30]. Though this basic CF is related to the explicand, it is usually unrealistic and violates the *Data manifold closeness*.

Distinctively, GradCF satisfies all three describable properties, which correlates with the explicand and stays on the manifold of counterfactual data. In other words, the generation of GradCF simultaneously implies the closeness to feature manifolds of explicand and counterfactual.

MNIST examples: Fig. 6a demonstrates the significance of *Explicand relevance*. Using digitals 7 as the references, we explain shifted digitals 1 at different positions. To human intuition, the critical areas distinguishing digital 1 to 7 are at the top left of digital 1 (see the red boxes). Fig. 6a shows that the highlighted areas of IG^2 are synchronized with the shift of explicands and critical areas, that is *Explicand relevance*.

As for Expected IG, using reference samples as baselines only provides the naive pixel contrast at the input feature

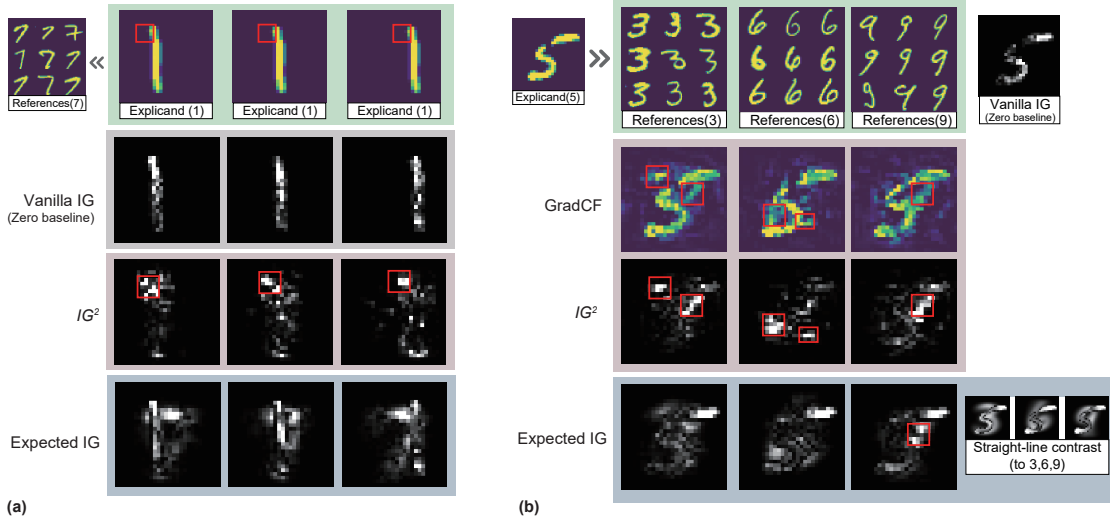


Fig. 6: Feature attributions of MNIST samples. (a) Shifted digital 1s explained with the references of digitals 7. (b) Digitals 5 explained with the references of different categories (digitals 3, 6, 9). The *most* critical areas that distinguish the explicand to reference are marked by red boxes, e.g., the explained digitals 1 will become digital 7 if we filled these areas. IG² is compared with Vanilla IG (using black baseline) and Expected IG (using references as the baselines).

space. This will result in explanations that are irrelevant to the explicand, which is obviously inconsistent with the intuition (see the last rows in Fig. 6).

Fig. 6b shows the impact of the different references, where the critical areas are marked by red boxes. Attributed to the gradients of counterfactual classes, the GradCF and IG² significantly highlight the critical areas of all three references. Due to the same issue of straight paths, attributions of Expected IG are overly focused on the upper right corners of digital 5, which is not the *most* critical areas⁵. As for IG with the all-black baseline, any pixels out of the explained digitals will not have the attributions, which is incomplete for the explanation.

In Section 7.1, we will further demonstrate the effects of counterfactual references on IG² with multiple datasets.

4.3 Axioms of IG²

Works [17], [9], [12] claimed that path methods are the unique methods that satisfy certain desirable axioms. As a subset of path methods, we justify IG² satisfies the following four axioms: *Completeness*, *Dummy*, *Implementation Invariance* and *Symmetry*, and GradCFE also satisfies the latter three.

Definition 4. (Completeness) For every explicand x , and baseline x' , the attributions ϕ_i add up to the prediction difference $f(x) - f(x')$:

$$\phi_i = f(x) - f(x'). \quad (9)$$

Remark 1. Like other path integral methods, IG² also integrates the gradient in a conservative (input) vector field. Since all the path methods satisfy Completeness regardless of the path shape (see [9], [31]), IG² satisfies Completeness.

Due to our proposal utilizing the model representation, we extend the definitions of the three remaining axioms to

⁵The ablation study is conducted in Appendix Section B.1 for validating the most critical areas that distinguishes digital 5 to digitals 3, 6, 9.

the representation layer version, the extension of which is respectively (i.e., resp.) shown in the brackets. Notably, if we use the output layer as representation, no extension is needed.

Definition 5. (Dummy) Dummy features get zero attributions. A feature i is dummy in a function f (resp. \tilde{f}) if for any two values x_i and x'_i and every value $x_{N \setminus i}$ of the other features, $f(x_i; x_{N \setminus i}) = f(x'_i; x_{N \setminus i})$ (resp. $\tilde{f}(x_i; x_{N \setminus i}) = \tilde{f}(x'_i; x_{N \setminus i})$). Conceptually, the feature that is not referenced by the model naturally requires zero attributions.

Remark 2. IG² satisfies Dummy and GradCFE satisfies Dummy at the representation layer. The latter is a sufficient condition for the former.

Proof. According to Eq. 5, given any point $\gamma^G(\alpha)$ on Grad-Path, the change on feature $\gamma^G(\alpha)_i$ is proportional the normalized gradient:

$$\Delta \gamma^G(\alpha)_i \propto \frac{\partial \|\tilde{f}(\gamma^G(\alpha)) - \tilde{f}(x^r)\|_2}{\partial \gamma^G(\alpha)_i} \times \frac{1}{W} \quad (10)$$

$$= \lim_{h \rightarrow 0} \left(\partial \|\tilde{f}(\dots, x_i + h, \dots) - \tilde{f}(x^r)\|_2^2 - \|\tilde{f}(\dots, x_i, \dots) - \tilde{f}(x^r)\|_2^2 \right) \times \frac{1}{hW}. \quad (11)$$

Based on the definition of Dummy, $\tilde{f}(\dots, x_i + h, \dots) \equiv \tilde{f}(\dots, x_i, \dots)$, so that

$$\Delta \gamma^G(\alpha)_i \equiv 0. \quad (12)$$

According to the definitions in Eq.3 and Eq. 6, we get the zero attributions of both IG² and GradCFE for dummy features at the representation layer.

The Dummy axiom of IG² does not require the feature to be dummy at the representation layer. Suppose the feature is dummy only for the model output (unextended definition). In that case, IG² still assigns zero attribution on this feature, the proof of which is similar (explicand's gradient

for dummy features in Eq. 3 constantly equals to zero) and not repeated here. \square

Definition 6. (Implementation Invariance) *Two networks are functionally equivalent if their outputs (resp. representations) are equal for all inputs, despite having very different implementations. Attribution methods should satisfy Implementation Invariance, i.e., the attributions are always identical for two functionally equivalent networks and do not refer to implementation details.*

Remark 3. IG^2 and GradCFE satisfy Implementation Invariance. The former is a sufficient condition for the latter. IG^2 and GradCFE only relies on the function gradients of output and representation (GradCFE only concerns representation gradient), which are invariant to the models' internal implementation before the representation layer.

Definition 7. (Symmetry) *For every function f (resp. \tilde{f}) is symmetric in two variables i and j , if $f(\dots, x_i, x_j, \dots) = f(\dots, x_j, x_i, \dots)$ (resp. \tilde{f}). If the explicand x are such that $x_i = x_j$, the attributions of symmetric function for features i and j should be equal. Conceptually, under the symmetric function, the identical symmetric variables receive identical attributions.*

Remark 4. IG^2 and GradCFE preserve Symmetry. The former is a sufficient condition for the latter. Notably, previous path methods are symmetry requires the variable i and j of the baseline x' are also identical, $x'_i = x'_j$, while our methods do not. The explicand with identical symmetric variables will consequently lead to the identical symmetric variables in the synthesized baseline GradCFE.

Proposition 1. (Guided IG [23]) *If the values of symmetric variables are equal at every point of the integration path, then their attributions are equal. Therefore, such a path attribution method is symmetry preserving.*

Proof. According to Proposition 1, IG^2 and GradCFE preserve Symmetry if the values of symmetric features on GradPath γ^G are equal at every point, the proof of which is in the following.

Given explicand x , we only focus on the symmetric variables i and j , $x = (\dots, x_i, x_j, \dots)$, where $x_i = x_j$. According to Eq. 5, the change on variable x_i along GradPath γ^G is:

$$\Delta x_i = -\frac{\partial \|\tilde{f}(\gamma^G(\alpha)) - \tilde{f}(x^r)\|_2^2}{\partial x_i} \times \frac{\eta}{W} \quad (13)$$

$$= (\tilde{f}(\gamma^G(\alpha)) - \tilde{f}(x^r)) \times \frac{-2\eta}{W} \times \frac{\partial \tilde{f}(\gamma^G(\alpha))}{\partial x_i} \quad (14)$$

$$= \lim_{h \rightarrow 0} \frac{\tilde{f}(\dots, x_i + h, x_j, \dots) - \tilde{f}(\dots, x_i, x_j, \dots)}{\partial h} \times \frac{-2\eta}{W} \times (\tilde{f}(\gamma^G(\alpha)) - \tilde{f}(x^r)). \quad (15)$$

and similarly, we can get the change on variable x_j :

$$\Delta x_j = \lim_{h \rightarrow 0} \frac{\tilde{f}(\dots, x_i, x_j + h, \dots) - \tilde{f}(\dots, x_i, x_j, \dots)}{\partial h} \times \frac{-2\eta}{W} \times (\tilde{f}(\gamma^G(\alpha)) - \tilde{f}(x^r)). \quad (16)$$

Because \tilde{f} is symmetric for variable i and j :

$$\tilde{f}(\dots, x_i + h, x_j, \dots) = \tilde{f}(\dots, x_i, x_j + h, \dots), \quad (17)$$

two gradients in Eq. 15 and Eq. 17 are equal and we get the identical changes on variable i and j :

$$\Delta x_i = \Delta x_j. \quad (18)$$

Starting from the identical value $x_i = x_j$ of the explicand, we can get the symmetric variables x_i and x_j are equal at every step of GradPath. Thus, both IG^2 and GradCFE provide identical attribution for the symmetric variables. \square

5 RELATED WORKS

This section first introduces the previous attribution methods in the field of XAI, and then systemically contrasts our proposal with the related works in three sub-fields: path attribution, Shapley values and adversarially counterfactual explanation.

5.1 Feature attribution

Feature attribution is a post-hoc method that explains AI models by scoring the feature contributions to the model output [32].

Gradient-based methods are widely used for attribution. One of the earliest successful work is DeconvNet [33], which applies a ReLU non-linearity to the gradient computation. Based on Vanilla Gradient [4] and DeconvNet, Guided Backpropagation [6] introduced an additional guidance signal from the higher layers. Furthermore, Class Activation Map (CAM) was developed [34] and its variants like Grad-CAM [5] also achieved success.

Another class of attribution methods is based on perturbation, which analyses the model sensitivity by perturbing the input features. Occlusion sensitivity maps [33] was one early method, which perturbs the input image with grey squares and observes the model prediction. Not restricted to deep models, LIME [35] can be applied to any prediction model by training a linear proxy model.

Shapley values can be considered a particular example of perturbation-based methods and is justified to be the unique method that satisfies certain desirable axioms [36]. However, computing the exact Shapley value is NP-hard [37], which is prohibitive for deep neural networks. Thus, the related works are dedicated to efficiently approximating the Shapley values with fewer model evaluations. Some works are based on sampling: Strumbelj et al. [38] and Mitchell et al. [39] respectively proposed Monte Carlo and quasi-Monte Carlo for randomly sampling permutations; KernelSHAP [12] used LIME to reduce the number of samples; Chen et al. [40] leveraged the underlying graph structure for the structured data; Wang et al. [41] took the advantages of contributive cooperator selection; Ancona et al. [42] introduced probabilistic deep network to approximately propagate the Shapley value through the network layers. To further accelerate the approximation, FastSHAP [43] trained a surrogate model to fast generate the explanation, which avoids the expensive sampling procedures; DeepSHAP [12] approximated the Shapley value at each layer and merged them by DeepLIFT [7] in a backward fashion.

5.2 Path methods

Path method is a popular feature attribution that integrates the gradients along a path. Table 1 has summarized the existing path methods to the best of our knowledge. IG² is the first path method with both model-specific path and baseline.

Contrasting Blur IG [24] Blur IG resembles IG² in using an iterative algorithm to simultaneously construct the baseline and the integration path. The nature of Blur IG is to iteratively build a path from the explicand to the baseline of a totally blurred explicand. Since the blurred baseline fully depends on the explicand, it lacks the counterfactual information within the model and data distribution. Moreover, Blur IG is restricted to images and not applicable to tabular data.

Contrasting Expected IG [19] Expected IG uses the informative baselines from the data distribution, which is the reference of our proposal. Nevertheless, the baseline is irrelevant to the explicand, and its straight-line path naively contrasts the baseline and explicand by the difference in the feature space, which still suffers from the saturation effects and noise problem. Notably, the Expected IG² (in Section 7.1.1) follows the Expected IG’s idea to calculate average attributions by sampling references from the data distribution.

Contrasting Guided IG [23] Guided IG is one close work to IG². Firstly, our proposal implies a similar motivation of Guided IG (discussed in Section 4.1). Second, both integration paths are iteratively calculated based on the gradient information to explicitly or implicitly avoid the saturated area. We argue that the shape of GradPath is a generalization of Guided IG’s path. If using ℓ_1 normalization in Eq. 21, the GradPath has the identical shape as Guided IG’s. We select the sparse features with the largest counterfactual gradients, while Guided IG selects the smallest explicand’s gradients in the converse direction (the identical shape does not guarantee the identical integration path).

5.3 Shapley values

IG methods are the generalization of Aumann-Shapley value, an extension of Shapley value to the continuous setting, which inherits desirable attribution axioms [9]. Compared with the sampling-based Shapley value approximations, IG² mainly advances in two aspects:

- **Scalability:** Though recent algorithms can achieve efficient approximations, they are still prohibitive for the high-dimensional input features (e.g., ImageNet samples). They have to apply the superpixel (group pixels) to reduce the input dimension [39], [42], [12], which impairs the explanation quality. On the large models, IG-based methods are much more efficient than most Shapley value algorithms, the computational time comparison to sampling-based KernelSHAP is reported in Appendix A.5.
- **Implicit zero baseline:** Similar to Vanilla IG, many Shapley value methods need to indicate the absence of features by replacing them with zero value, which implicitly defines a zero baseline. The zero baseline’s adverse effects on feature attributions have been discussed in the previous sections.

TABLE 2: Evaluation of attribution methods on XAI-BENCH

	fai.(↑)	mon.(↑)	ROAR(↑)	G-S(↑)	inf.(↓)
Random	-0.033	0.458	0.332	-0.060	0.034
Vanilla IG	0.349	0.440	0.356	0.714	0.015
Guided IG	0.342	0.463	0.359	0.681	0.021
Expected IG	0.596	0.470	0.365	0.814	0.014
DeepSHAP	0.380	0.488	0.357	0.821	0.014
KernelSHAP	0.370	0.435	0.340	0.901	0.015
IG²(Ours)	0.610	0.486	0.377	0.833	0.021

* fai.:faithfulness mon.:monotonicity G-S:GT-Shapley inf.:infidelity

Contrasting DeepSHAP [12] Unlike other sampling-based approximations, DeepSHAP is more related to IG methods. Its core part, DeepLIFT, replaces the gradient at each nonlinear function with its average gradient, which is shown to be most often a good approximation of IG [44].

In summary, though sharing the same theory fundamental, we argue that IG and Shapley value approximations are on two different tracks: the former is mainly designed for explaining large networks with accessible gradients, and the latter is for accurately approximating the exact Shapley value, which is more suitable for the small black-box models.

5.4 Adversarially counterfactual explanation

The adversarial learning shares the same optimization objective with counterfactual explanation, and they are tightly related [30]. Some works [45], [46] utilized adversarial attack to explain the network. GradCF differs from counterfactual explanation and adversarial attack in violating the principle that counterfactual explanation should be the small perturbation on the explicand [28]. Hence, we argue that GradCF is neither a canonical counterfactual explanation (GradCF still provides a counterfactual explanation) nor an adversarial attack.

From the perspective of methodologies, the iterative gradient descent optimization method in Eq. 4 follows the adversarial attack method. The optimization with ℓ_2 normalization is from projected gradient descent (PGD) [29] while ℓ_1 normalization is from sparse adversarial attack [47]. The only difference is that adversarial attack methods clamp the computed instance within the neighborhood of explicand to guarantee imperceptible perturbations.

Notably, the same ℓ_2 normalized optimization method is also used in work [48]. Nevertheless, they focus on searching the robust features under the adversarial attack while the model explanation is out of their scope.

6 EXPERIMENTS

We conduct the attribution experiments on one synthetic dataset, XAI-BENCH, and four real-world tasks: image classification on ImageNet, question classification on TREC, anomaly classification on wafer map failure pattern, and face attribute classification on CelebA. We compare IG² with six methods:

- **(Vanilla) Gradient:** The fundamental feature attribution method based on backpropagation, using the

TABLE 3: Evaluation of attribution methods on real-world datasets

Datasets	Explainers	Ground truth		SIC AUC	
		AUC \uparrow	SUM \uparrow	ADD \uparrow	DEL \downarrow
ImageNet	Gradient	0.482	0.336	0.467	0.209
	Vanilla IG	0.536	0.327	0.476	0.205
	Guided IG	0.599	0.464	0.545	0.212
	Expected IG	0.666	0.431	0.557	0.116
	DeepSHAP	0.694	0.470	0.543	0.206
	KernelSHAP	0.747	0.498	0.561	0.274
	IG²(Ours)	0.805	0.516	0.656	0.115
TREC	Gradient			0.909	0.189
	Vanilla IG			0.937	0.159
	Guided IG			0.938	0.156
	Expected IG	—*		0.940	0.141
	DeepSHAP			0.933	0.170
	KernelSHAP			0.933	0.172
	IG²(Ours)			0.942	0.140
Wafer map	Gradient	0.570	0.226	0.661	0.216
	Vanilla IG	0.732	0.342	0.829	0.061
	Guided IG	0.758	0.450	0.789	0.050
	Expected IG	0.850	0.488	0.883	0.038
	DeepSHAP	0.863	0.528	0.890	0.029
	KernelSHAP	0.683	0.339	0.707	0.042
	IG²(Ours)	0.849	0.551	0.898	0.036
CelebA \dagger	Gradient	0.748	0.211	0.745	0.296
	Vanilla IG	0.705	0.175	0.740	0.314
	Guided IG	0.653	0.225	0.744	0.370
	Expected IG	0.698	0.189	0.737	0.293
	DeepSHAP	0.699	0.179	0.750	0.309
	KernelSHAP	0.788	0.212	0.765	0.197
	IG²(Ours)	0.795	0.224	0.815	0.205

* The ground truth of TREC is not available.

\dagger The ground truth of CelebA face attributes is generated by face parsing model pretrained on CelebAMask-HQ [49], which is detailed in Appendix B.6.

input gradient w.r.t. the model’s prediction for generating the saliency maps.

- **Vanilla IG, Guided IG, Expected IG:** Three IG-based methods, which have been discussed in the previous sections.
- **KernelSHAP:** A basic sampling method for approximating Shapley values of black-box models, which is a common baseline for approximation algorithms. Due to the scalability limitation, the superpixel technique is applied when attributing ImageNet and wafer map samples with KernelSHAP.
- **DeepSHAP:** A high-speed Shapley value approximation for deep models based on DeepLIFT.

For the baselines of compared methods, Vanilla IG, KernelSHAP, and Guided IG all use the black image as the (implicit) baseline, Expected IG and DeepSHAP samples the baselines from the same distribution as the counterfactual references of IG².

6.1 XAI Benchmark

First, we evaluate our proposal on the synthetic datasets and metrics released by XAI-BENCH [50], a benchmark for feature attribution algorithms. Synthetic datasets allow the efficient computation of the ground truth Shapley values and other metrics, which is intractable on real-world datasets. We briefly introduced the dataset and metrics, the details of which can be found in the XAI-BENCH work [50].

6.1.1 Synthetic Dataset

The features are sampled from a multivariate normal distribution $\mathbf{X} \sim \mathcal{N}(\mu, \Sigma)$, where μ is the mean vector and Σ is the covariance matrix. The labels are binary (0 and 1) and defined over a *piecewise* distribution with the function $\Psi(x)$. The explained model is a trained three-layer perceptron for the regression task on the synthetic dataset. The specification of the model and synthetic dataset are reported in Appendix B.2.

6.1.2 Metrics

We use five metrics from XAI-BENCH: (1) *faithfulness* computes the Pearson correlation coefficient between the attribution and the approximate marginal contribution for each feature; (2) *monotonicity* computes the fraction of the marginal improvement for feature with attribution order i is greater than the marginal improvement for feature with attribution order $i + 1$; (3) *ROAR* is remove-and-retrain, which retrains the model with the features removed and the area-under-the-curve (AUC) of the model is computed; (4) *GT-Shapley* computes the Pearson correlation coefficient of the feature attribution to the ground-truth Shapley values (ground-truth marginal improvement); (5) *Infidelity* is computed by considering the effects of replacing each feature with a noisy baseline conditional expectation.

6.1.3 Results

Table 2 reports the five metrics for evaluating the feature attributions on XAI-BENCH datasets. The Vanilla IG and Guided IG use zero baselines with different paths, and the Expected IG uses data distribution as the baseline. We also use the randomly generated attribution (Random) as a weak comparison.

The results evaluate the feature attributions of the small model and low input dimensions. IG² generally outperforms most other methods on the first three metrics. Unsurprisingly, the Shapley value sampling method (KernelSHAP) achieves the best performance on the GT-Shapley metric. The improvement of Expected IG over other IG methods reveals that using the exception of attribution from the data distribution baseline is effective.

6.2 Metrics for real-world datasets

We adopt two types of quantitative metrics for evaluating the feature attribution on real-world datasets:

Ground truth annotation [51] The first metric requires the ground truth segmentation annotated by humans. The better attribution should be closer to the ground truth annotations. Specifically, this metric treats the attributions as binary classification prediction scores. With changing the threshold of attribution scores to be negative class, the

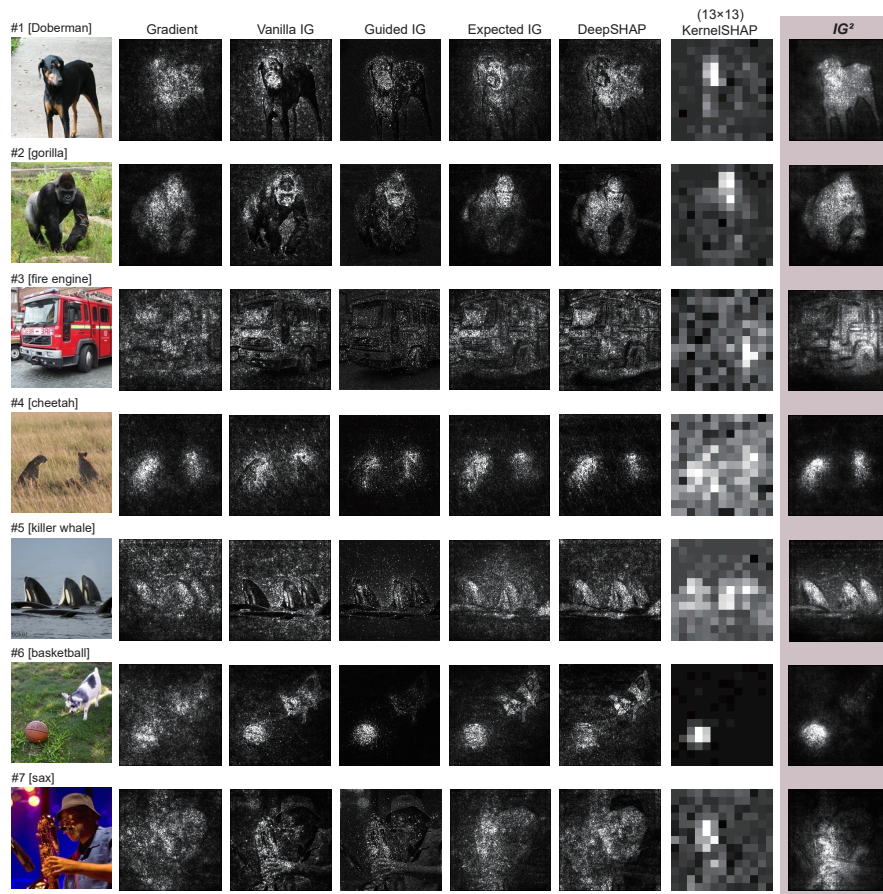


Fig. 7: Feature attributions on images from ImageNet dataset. The predicted classes are listed in square brackets.

area under the receiver operating characteristic curve is calculated [23], which is called *ground truth-AUC*. We can also use the multiplication of (normalized) attribution scores and ground truth to show the sum of attributions on the annotated features, which is called *ground truth-SUM*.

Softmax Information Curve (SIC AUC) [26] This metric is free from the ground truth annotation and measures how much the attributed features can influence the model prediction, which is similar to the marginal contribution concept in the Shapley theory. The better attribution should have a better focus on where the model is truly looking. There are two metrics in different directions. The first one gradually adds the feature values of the explicand to the background. By sliding an attribution threshold, the feature with the largest attribution is first added and the least the last. The better attribution method should increase the model prediction more quickly, which can be quantized by the area under the Softmax prediction curve w.r.t threshold, *SIC AUC-ADD*. Conversely, another metric deletes the most important feature until all the features are replaced by the background [19]. Similarly, the better attribution method should decrease the model prediction quicker, where the AUC w.r.t. threshold is called *SIC AUC-DEL*.

Table 3 summarizes four metrics of three real-world datasets, where IG^2 significantly outperforms other methods in general.

6.3 Image classification explanation

6.3.1 Dataset

We validate IG^2 on a standard image classification dataset, ImageNet. We take the explained images from the ILSVRC [21] subset (1k classes) with the ground truth annotations. We use the pre-trained classifier of Inception-v3 [22] with input size 299×299 . We only consider the images that are predicted as one of the top 5 classes by the Inception-v3 classifier.

6.3.2 Attributions

Fig. 7 shows ImageNet images explained with four IG-based methods and two Shapley value methods, where IG^2 generally outperforms previous techniques. Whereas guided IG efficiently reduces the noises by constructing the path that avoids the saturated areas (discussed in Section 4.1), it gives incomplete attributions due to the zero baseline, which is also a drawback of Vanilla IG and KernelSHAP. This problem is especially evident in the images with black subjects (images #1, #2, #4, and #5 in Fig. 7).

Expected IG and DeepSHAP achieve similar attribution results. They mitigate the incomplete attribution problem by introducing informative baselines providing more attributions on image subjects, but it still suffers from the undesirable noise problem. This is especially obvious in the images with interference objects (e.g., the dog in #6[basketball] and the player in #7[sax]). Expected IG and DeepSHAP will incorrectly highlight these objects, which are irrelevant to the explicand class label.

IG² combines two advantages of Guided IG and Expected IG, respectively attributed to two techniques, GradPath and GradCF:

Less noise by GradPath: As discussed in Section 4.1, the integration path of IG² successfully mitigates the saturation effects. Image attributions in Fig. 7 also validate this superiority. IG² provides significantly less noisy attributions (less noise on background or irrelevant objects) over IG and Expected IG that use the straight-line path. Compared with Guided IG, IG² is competitive and slightly better on some samples (e.g., image #7).

More complete attribution by GradCF: As discussed in Section 4.2, the explicand-specific GradCF of IG² can highlight the critical features that distinguish the explicand from the counterfactual reference. As for images from ImageNet, the critical areas should be the subjects of the explicand label. Appendix Fig. B.6 shows the difference between the explicand and GradCF (i.e., GradCFE). Based on this counterfactual contrast, IG² attributions highlight the critical features more completely than IG, Guided IG, and even Expected IG.

Table 3 with quantitative metrics shows our proposal achieves the best performances. Despite the incomplete attributions, the features highlighted by Expected IG are enough to make the classifier give incorrect predictions. This is why Expected IG achieves comparable SIC AUC-DEL value to IG², but got much worse performances on SIC AUC-ADD and ground truth metrics, which are more dependent on attribution completeness. Since the superpixel technique makes the high attributions concentrated on small areas, KernelSHAP achieves relatively good performance on metrics about ground truth annotation, but its SIC AUC metrics are not desirable.

6.4 Question classification explanation

6.4.1 Dataset

In the field of natural language processing (NLP), question answering is an important task. Question classification can categorize the questions into different semantic classes (whether the question is about location, person or numeric information, etc.), which can impose constraints on potential answers. For instance, the question—“Where did guinea pigs originate?” should be classified as having the answer type [location].

We use TREC question dataset [52] involving six semantic classes and train a CNN-based classifier (TextCNN) [53]. We attribute word-level features in order to seek the trigger words that contribute most to the answer type.

6.4.2 Attributions

Fig. 8 lists questions sampled from five classes from TREC dataset with word attributions by IG² and IG. IG uses the all-zero embedding vector as the baseline. Compared to IG, the trigger words highlighted by IG² are more consistent with human grammatical perception. We summarize two advantages of IG² over IG.

Less attributions on weak interrogative words: Some initial interrogative words are strongly associated with the question types, e.g., “where” indicates the question for [location] and “who” indicates [human] (see questions #2 and #7

Question #	Class	IG ² Attribution	IG Attribution
#1	[LOCATION]	What are the only two states that incorporate the Confederate battle flag in their flags ?	What are the only two states that incorporate the Confederate battle flag in their flags ?
#2	[LOCATION]	Where did guinea pigs originate ?	Where did guinea pigs originate ?
#3	[ENTITY]	Which drug is commonly used to treat AIDS ?	Which drug is commonly used to treat AIDS ?
#4	[ENTITY]	What was the name of the Protestant revolt against the supremacy of the Pope ?	What was the name of the Protestant revolt against the supremacy of the Pope ?
#5	[DESCRIPTION]	What is the difference between microprocessors & microcontrollers ?	What is the difference between microprocessors & microcontrollers ?
#6	[DESCRIPTION]	How do you make panoramic sugar eggs for Easter - the ones with the scene inside ?	How do you make panoramic sugar eggs for Easter - the ones with the scene inside ?
#7	[HUMAN]	Who sought to create The Great Society ?	Who sought to create The Great Society ?
#8	[HUMAN]	What are the characters' names in the Scooby-Doo cartoon ?	What are the characters' names in the Scooby-Doo cartoon ?
#9	[NUMERIC]	What are the lengths of pearl necklaces ?	What are the lengths of pearl necklaces ?
#10	[NUMERIC]	How long does it take the typical hen to lay 19 dozen eggs ?	How long does it take the typical hen to lay 19 dozen eggs ?

Fig. 8: Word attributions for questions from TREC dataset. IG² is compared with Vanilla IG. The color depth indicates attribution strength, and the color type indicates the attribution direction (red is negative, and green is positive). The predicted classes are listed in the top of each question. The complete attributions of all methods are reported in Appendix Fig. B.8.

in Fig. 8). In this case, these interrogative words should be strongly attributed.

On the other hand, some interrogative words are weakly related. For instance, “what” and “which” may indicate almost all the question types (questions #1, #3, #4, #5, #8, and #9). Word “how” itself is ambiguous, which becomes a trigger phrase only when combined with other words (#6 and #10). These weakly related interrogative words should be less attributed.

Shown in Fig. 8, Vanilla IG strongly attributes all the interrogative words, whereas IG² precisely attributes different interrogative words. IG² keeps large attributions on strong interrogative words (“where” and “who” in questions #2 and #7), and provides much less attributions on weak interrogative words (the remaining questions).

More attributions on critical phrases: Compared with IG, attributions of IG² concentrate more on the critical phrases, such as, “drug” and “name revolt” for [entity] (questions #3 and #4), “how do” for #6[description], “sought to” for #7[human], and “lengths” for #9[numeric].

Table 3 validates that word attributions of IG² are more consistent with the model behavior than other methods. Since the number of input features in TREC dataset is small (maximum 37 words), sampling-based KernelSHAP is competitive with other path methods.

6.5 Wafer map failure pattern explanation

6.5.1 Dataset

Wafer map analysis is critical in daily semiconductor manufacturing operations. Wafer maps provide visual details

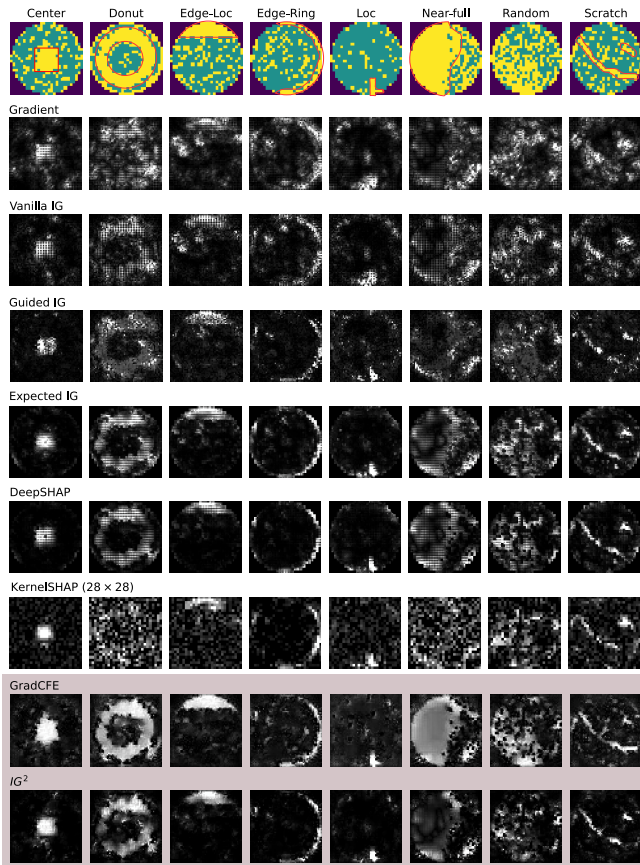


Fig. 9: Feature attributions on wafer maps with eight different failure patterns. The first row shows the original anomaly wafer maps with the red ground truth annotation based on expert knowledge.

that are crucial for identifying the stage of manufacturing at which wafer pattern failure occurs. Instead of manual work, automatically identifying different types of wafer map failure patterns can effectively improve the efficiency of the semiconductor manufacturing process.

The explanation of classification deep neural network for wafer map failure pattern can determine which parts (pixels) of the wafer maps are the cause that leads to the failure. This explanation enhances the model’s ability to automatically identify the cause of the anomaly wafer maps rather than only recognizing the failure types.

Specifically, we use WM-811K dataset [25], which is the largest known wafer map dataset available to the public. We use a subset of the whole dataset for training the classification model based on convolution neural networks (CNN), achieving a classification accuracy greater than 98.5% on both train and test sets. The implementation detail of the classification model and sampled instances from WM-811K are provided in Appendix B.5.

6.5.2 Attributions

First of all, Fig. 9 directly compares the different attributions on eight samples with different patterns in WM-811K dataset. Compared to naive gradient methods, integrated gradients significantly improves feature attribution. Still, the Vanilla IG fails to completely highlight the failure patterns (as the red ground truth) and suffers from the noise

problem. Though Guided IG efficiently reduces the noise on the irrelevant features by the designed path, its attribution is still incomplete, caused by the arbitrary baseline containing less counterfactual information. Expected IG and DeepSHAP solve this by using the informative baselines over the data distribution of [nonpattern] instances, but its straight-line path still introduces some noises (especially on the circle edges).

Our GradCFE solves the inaccurate counterfactual information problem in the existing baselines, shown by GradCFE. It highlights the features contributing to the model representation difference between the explicand and reference. However, it simultaneously accumulates lots of undesirable noises on irrelevant features. IG^2 successfully solves this side effect by incorporating the gradient of explicand’s prediction, which significantly reduces the noise attributions by filtering out the features that have less contribution to the output of explicand’s class.

Overall, compared with the advanced existing attribution methods, IG^2 provides less noisy attributions that are most consistent with expert knowledge and human intuition. Moreover, Table 3 reports quantitative metrics to evaluate the attributions. The results show that IG^2 generally outperforms other advanced path attribution methods and KernelSHAP. Our proposal significantly improves the Vanilla IG’s performance and is competitive with Expected IG and DeepSHAP.

6.6 Face attribute classification explanation

6.6.1 Dataset

Each face image in CelebA [54] has 40 binary face attribute labels, indicating the presence or absence of specific facial attributes like smiling, wearing earrings, or having a mustache. We train the face attribute classification model on the CelebA dataset, based on MobileNet-v2 [55] with 40 output nodes corresponding to each face attribute. The classification accuracy for each face attributes are reported in Appendix B.6.

For multi-label classifier, we separately explains each output label, i.e., one face attribute at a time [16]. We use the counterfactual references that are most relevant to the explicand, i.e., the faces with labels differ in the explained attribute but are closet in other face attributes. The effect of references on CelebA will be analyzed in Section 7.1.4.

6.6.2 Attributions

Fig. 10 showcases the feature attributions on the CelebA face images. The effectiveness of a feature attribution method is determined by its ability to accurately emphasize the image region associated with the explained label (as indicated by red dashed line areas in Fig. 10). Using face image with label [Black_Hair] as a case study, IG^2 method demonstrates a more focused attribution towards the hair region, with less noises than other methods. Conversely, Vanilla IG and Guided IG encounter issues with black baselines in face images, mistakenly ignoring black pixels. Although Vanilla Gradient and Expected IG methods show relatively good performance on CelebA datasets, they still suffer from the saturation effect, leading to undesirable attributions on the irrelevant pixels, such as the image background.



Fig. 10: **Feature attributions on CelebA face attributes.** The explained labels appear at the top of each explicand. The critical facial areas associated with the explained label are marked in red dashed lines. The feature attributions are shown as the heatmaps on the images, where warmer colors (reds and yellows) denote areas of higher importance.

Overall, the attributions by IG^2 method are more precisely aligned with the facial regions that are relevant to the explained labels, whereas other methods tend to produce noisier and less accurate attributions on the critical facial regions.

6.7 Ablation study

Furthermore, based on the wafer map dataset, we studied the impact of GradCF and GradPath independently as the baseline and integration path for path methods. Table 4 reports three different baselines (black, train data, and GradCF) under three different paths (straight-line, Guided IG 's, and GradPath). As a baseline under the straight-line path and Guided- IG 's path, GradCF achieves the best performance of most metrics compared with the other two. On the other hand, GradPath outperforms than other two paths with the GradCF baseline.

In general, we can conclude that: (1) GradCF is a good baseline for path attribution, even independently combined with other paths. (2) GradPath outperforms other paths on the GradCF baseline, which accomplishes IG^2 .

TABLE 4: Ablation study of GradCF and GradPath

Paths	Baselines	Ground truth		SIC AUC	
		AUC \uparrow	SUM \uparrow	ADD \uparrow	DEL \downarrow
Straight-line	Black	0.732	0.342	0.829	0.061
	Train data	0.810	0.445	0.777	0.053
	GradCF	0.845	0.510	0.842	0.041
Guided- IG 's	Black	0.758	0.450	0.789	0.050
	Train data	0.804	0.493	0.775	0.043
	GradCF	0.781	0.472	0.819	0.037
GradPath (IG^2)	GradCF*	0.849	0.551	0.898	0.036

* The baseline of GradPath is iteratively synthesized, so only GradCF is available for GradPath.

7 IMPLEMENTATION DETAILS

We discuss the details of IG^2 , including the reference, step, normalization, similarity measure, and computational cost. We provide in-depth analyses of different choices on these hyper-parameters. Some supplementary experiments are reported in Appendix A.

7.1 Reference

The choice of counterfactual reference is a major hyper-parameter of IG^2 . Specifically, IG^2 attributions are sensitive to the *category* of counterfactual reference (while relatively insensitive to different samples of the same category).

Choice of reference category: For the classification tasks on different datasets, the ways to sample references are also different:

- **Anomaly classification:** For the dataset consisting of anomaly and normal samples (e.g., wafer map failure patterns), it is natural to use the samples of the normal category as the references for the anomaly explicand rather than other anomaly categories.
- **General classification:** Most datasets do not have such a natural category for reference, such as ImageNet, TREC, etc. Without loss of generality, we randomly sample the references from the different categories. Empirically, we recommend uniformly sampling references from more categories and a few (1 or 2) samples per category.
- **Tricks for denoising:** During experiments, we find using the references of categories that are closely relevant to the explicand can reduce the noises in attributions, but at the cost of losing completeness. This will be beneficial for the explicands with interference terms, such as some ImageNet samples (Section 7.1.2) and multi-label CelebA samples (Section 7.1.4).

Notably, without loss of generality, we take the second one (without denoising tricks) as the default reference choice strategy. The effect of reference category on IG^2 attributions are discussed on four datasets, MNIST (Fig. 6), ImageNet (Section 7.1.2), TREC (Section 7.1.3), and CelebA (Section 7.1.4).

7.1.1 Expected IG^2 over references

To eliminate the influence of the reference choice and reduce noise, we use the expectation of IG^2 as the final attribution.

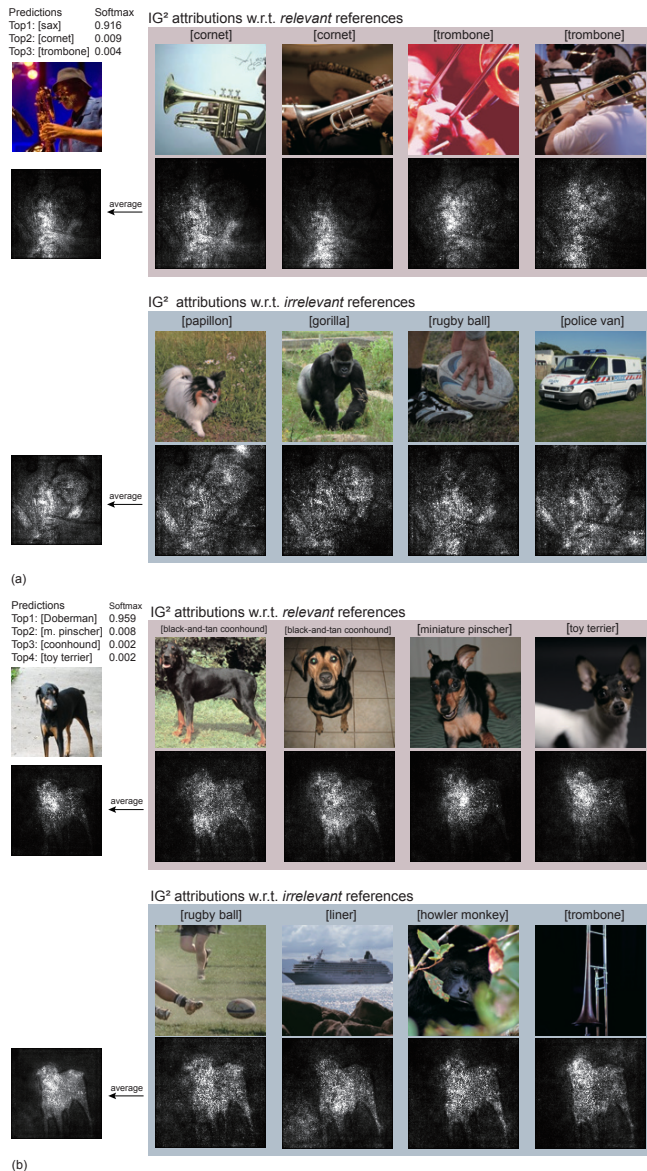


Fig. 11: Feature attributions w.r.t. different references. (a) Explained image of class [sax] with interference object “player”. (b) Explained image of class [Doberman] on pure background.

The Expected IG² is averaged over the references sampled from counterfactual categories, which is defined as:

$$\phi_i^{IG^2} = \mathbb{E}_{x_r \sim D^r} \phi_i^{IG^2}(x_r), \quad (19)$$

where D^r is the data distribution of the counterfactual categories to the explicand and $\phi_i^{IG^2}(x_r)$ is calculated by Eq. 3 as a function of x_r . In the following, we make no distinction between IG² and Expected IG², and use Expected IG² as the practice for experiments.

7.1.2 References of ImageNet

During experiments of ImageNet, we find that the category of reference can influence the IG² attributions. We categorize the references into two types by their labels: *relevant* references and *irrelevant* references. *Relevant* references are the samples of categories that are closely related to the

TABLE 5: Evaluation of IG² reference choice strategies on ImageNet

Strategy	Set of explicand	Ground truth		SIC AUC	
		AUC \uparrow	SUM \uparrow	ADD \uparrow	DEL \downarrow
Relevant	W/ interference	0.905	0.345	0.901	0.084
	Pure background	0.755	0.633	0.537	0.119
	Whole	0.798	0.551	0.641	0.109
Irrelevant	W/ interference	0.864	0.273	0.876	0.086
	Pure background	0.781	0.613	0.568	0.126
	Whole*	0.805	0.516	0.656	0.115

* The strategy reported in Table 3.

explicand, e.g., the classes in model top 3 predictions, and *irrelevant* references are the samples of other classes.

Generally, we find that only using *relevant* references will lead to more concentrated (less noisy) but less complete attributions. Contrarily, the *irrelevant* references can ensure the complete attribution covering the whole image subject but at the cost of introducing more noise. Fig. 11 and Appendix Fig. B.7 intuitively compares the IG² attributions w.r.t. different references. Moreover, we propose a trick to solve this trade-off in the choice of references.

Trick of reference choice: Empirically, the explicands with interference objects will be beneficial from the *relevant* references (see Fig. 11a and Appendix Fig. B.7a), the interference objects of which will be less attributed. Contrarily, the image with the explained subject on the pure background will be beneficial from the *irrelevant* references (see Fig. 11b and Appendix Fig. B.7b), where attributions on subjects will be more complete. This rule allows us to sample the references from particular categories to improve the attribution quality.

This trick is consistent with the intuition of counterfactual explanation: *the contrast between ambiguous (hard-to-identify) classes will highlight the most critical features of explicands*. Notably, this trick is only necessary for some explicands in specific datasets. In more general cases, we just need to sample the references uniformly from the counterfactual classes.

We conduct a quantitative evaluation for different reference choice strategies on the ImageNet dataset, the results of which are reported in Table 5. We split the explained samples into two subsets: One subset is with interference objects, and another one is on the pure background. We consider two strategies: “*Relevant*” selects references from the relevant categories of the top 4 predictions; “*Irrelevant*” randomly and uniformly samples references from other categories.

By the denoising trick (using relevant references), the attributions are more concentrated, which leads to higher *ground truth-SUM* and *SIC AUC-DEL* for all images. For the interfered images, all four metrics are significantly improved by this strategy. Since images on the pure background account for the majority in ImageNet ($\sim 72\%$ in our test set), the two reference choice strategies are competitive on the whole test set. Without loss of generality, on ImageNet dataset, IG² uses the strategy that randomly samples the references by default.

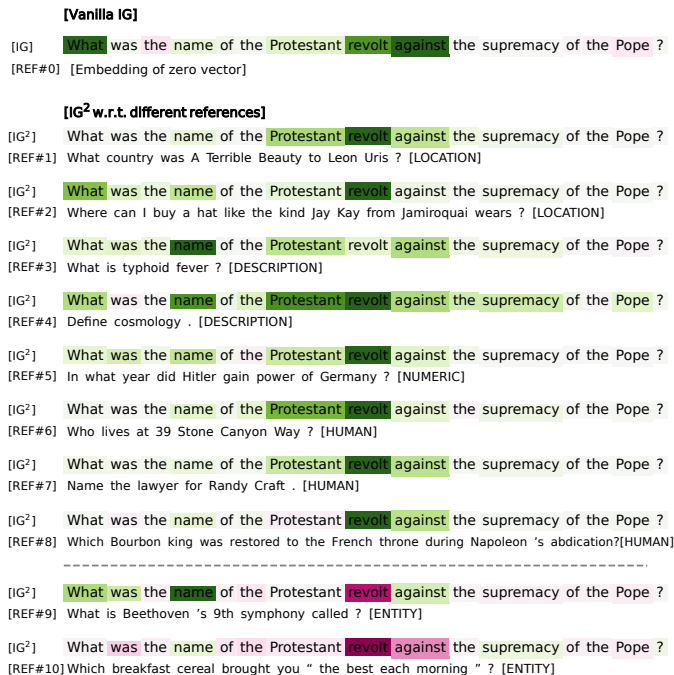


Fig. 12: Word attributions w.r.t. different references, for the question “What was the name of the Protestant revolt against the supremacy of the Pope?” of class [entity]. REFs #1 to #8 are used for calculating the Expected IG² reported in Fig. 8 #4.

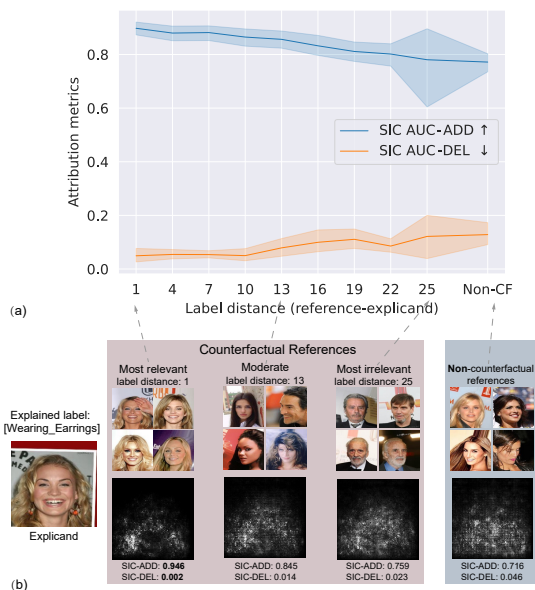


Fig. 13: (a) Curves of attribution metrics w.r.t. CelebA label distance between reference and explicand. (b) A CelebA example attributed by IG² of different references (explained label: [Wearing_Earrings]).

7.1.3 References of TREC

Fig. 12 lists IG² attributions w.r.t. different references, for the question #4 in Fig. 8. Fig. 12 intuitively shows that references of different categories provide different counterfactual contrast, which makes IG² explanation more in line with the human-authored grammar rules.

Based on grammar rules, the subject phrase of the ques-

tion #4 (of class [entity]) should be “name of revolt”. The two most attributed words by Vanilla IG are “what” and “against” (see REF #0 in Fig. 12), which are inaccurate since they do not determine the class [entity].

IG² uses references #1 to #8, where some insights can be found into the counterfactual explanation:

- Compared to IG, all the references make IG² have much less attribution on “what”, which is irrelevant to the class [entity]. Notably, even if the interrogative word of reference is not “what”, IG² attribution is still significantly reduced (see REFs #4 to #8).
- Almost all the counterfactual references contrastively highlight “revolt”, since modifying this word is the fastest way to turn the explicand into another class⁶. Reference #3 is an exception, an interpretation of which is: if we only modify the word “revolt”, the sentence will hardly become the class [description]; but if removing the phrase “the name of”, the explained question will be similar to reference #3.
- The word “name” is also more highlighted by IG², but the references of classes [human] and [location] do not provide this contrast. This is because the word “name” is also related to the classes [human] and [location] (e.g., “name of lawyer” and “name of country”).

Finally, REFs #9 and #10 in Fig. 12 list the attributions w.r.t. the references of the same class, where the word “revolt” is highlighted in the opposite direction. The attributions w.r.t. non-counterfactual references are confusing, which is why we only consider the references of different classes when we compute the Expected IG².

7.1.4 Reference of CelebA

We leverage a multi-label dataset to quantitatively evaluate the choice of references. Thus we can use the ℓ_1 distance of label vectors to measure the similarity between references and explicand, and then build the quantitative correlation between the reference categories and feature Attributions.

Fig. 13a reports the feature attribution metric curves w.r.t. label distances, averaged over 300 CelebA samples. Fig. 13b displays an explicand with the explained label [Wearing_Earrings], showing its attributions w.r.t. different references. The non-counterfactual references have the identical explained label to the explicand, and *vice versa*.

The results show, the similar counterfactual references (with small label distances) lead to better feature attributions (e.g., highlighting the earring pixels). Higher label distances result in a decline in the attribution metrics. The non-counterfactual references cannot contrast the explained label, which leads to the worst feature attributions.

Based on the results, we make two conclusions for the reference choice on the multi-label dataset: (1) References should be counterfactual on the explained label; (2) Using relevant references will benefit the feature attributions of multi-label samples. The second conclusion is consistent with the above denoising tricks for images with interference objects. In the multi-label classification, the not-explained labels (e.g., the face attributes other than [Wearing_Earrings])

6. For instance, replacing “revolt” with “country” turns the question into class [location], and replacing with “leader” turns into [human].

can be regarded as the interference objects, so relevant references will make the feature attributions less noisy and more concentrated on the explained image parts.

7.2 Step size and number

Appendix Fig. A.1 uses an ImageNet example to illustrate the effect of step size and number on IG^2 attribution. Appendix Fig. A.1a shows the objective loss (Eq. 4) curves during the optimization for GradPath, and Appendix Fig. A.1b shows IG^2 attributions w.r.t. different step sizes and numbers. The step sizes and numbers chosen for different datasets are reported in Appendix Table A.1.

Step size can affect the IG^2 attributions. There is a trade-off issue on step size: small step sizes tend to result in less noisy but incomplete attributions, whereas large step sizes result in complete but noisy attributions. This is intuitive: when the total magnitude is more limited, the perturbation will be concentrated on a few more important features. In practice, we will choose a moderate step size that can well balance these two sides.

Step number is not a critical hyper-parameter. Appendix Fig. A.1 shows that IG^2 attribution does not substantially change when objective loss approaches convergence. Hence, we set the step number to a relatively large value that can allow optimizations of most explicands to be converged.

7.3 Representation distance measure

IG^2 constructs GradPath and searches GradCF by minimizing the distance between model representations of reference and explicand. Eq. 4 shows this optimization objective, where the distance between two vectors is based on the Euclidean measure. The usage of Euclidean distance is inspired by the feature matching trick in GAN training [56] and the adversarial robustness work [48]. Besides, the Cosine similarity and ℓ_1 norm are two common measures for the vector distance. We conduct an ablation study to compare the different distance measures in IG^2 .

Appendix Table A.2 reports the performance gap between Cosine similarity and ℓ_1 norm to Euclidean distance, and Appendix Fig. A.4 displays ImageNet samples attributed by three different measures. Based on the quantitative and qualitative results, we argue that Euclidean distance is not significantly better than Cosine similarity, while ℓ_1 norm is not a good choice for IG^2 attributions. Empirically, IG^2 uses the Euclidean distance by default, achieving slightly higher evaluation metrics in experiments.

7.4 Computational cost

We analyze the computational cost of IG^2 . The major computational cost of path methods is gradient calculation. Since GradPath requires the same gradient calculation times as the gradient integration, IG^2 requires at least twice the computational cost over other methods. On the other hand, IG^2 commonly requires about 10 references to get the desired performance, while other methods only require one. Hence, the number of gradient calculations in IG^2 is about 20 times more than other methods.

In practice, we can reduce the running time by calculating the gradients of different references in one batch.

The practical running time of IG^2 is about 10 to 20 times that of (Expected) IG and about 3 times that of Guided IG. Appendix Table A.3 reports the average explanation time per sample of different methods. Despite the increased computational cost, the running time of IG^2 is still practically feasible. Compared with the sampling-based KernelSHAP method, even with superpixel techniques, IG^2 is significantly faster on the high-dimensional datasets.

Besides above hyperparameters, the discussions about normalization and representation layer are presented in Appendix A.2 and A.3

8 CONCLUSION

This paper proposes a novel feature attribution method, Iterative Gradient path Integrated Gradients (IG^2), which simultaneously incorporates two gradients, the explicand’s and counterfactual. IG^2 proposes two novel essential components of path methods: baseline (GradCF) and integration path (GradPath). GradPath incorporates the counterfactual gradient into its direction and implicitly solves the saturation effects and noisy attributions. GradCF is the first baseline that contains the information of both model and explicand, avoiding the previous arbitrary baseline choice.

We contrast our work with path methods and the works in the field of counterfactual explanation and adversarial learning. We argue that our work can be regarded as a generalization of Guided IG. We intuitively interpret our proposal and justify the desirable axioms of IG^2 in theory. The effectiveness of IG^2 is verified by an XAI benchmark and multiple real-world datasets from diverse domains with qualitative and quantitative results. Moreover, the ablation study reveals that GradPath and GradCF individually improve the attribution of IG methods, harmonized by IG^2 .

REFERENCES

- [1] X.-H. Li, C. C. Cao, Y. Shi, W. Bai, H. Gao, L. Qiu, C. Wang, Y. Gao, S. Zhang, X. Xue, and L. Chen, “A survey of data-driven and knowledge-aware explainable ai,” *IEEE Transactions on Knowledge and Data Engineering*, vol. 34, no. 1, pp. 29–49, 2022.
- [2] Y. Shen, C. Yang, X. Tang, and B. Zhou, “Interfacgan: Interpreting the disentangled face representation learned by gans,” *IEEE Transactions on Pattern Analysis and Machine Intelligence*, vol. 44, no. 4, pp. 2004–2018, 2022.
- [3] S. A. Bargal, A. Zunino, V. Petsiuk, J. Zhang, K. Saenko, V. Murino, and S. Sclaroff, “Guided zoom: Zooming into network evidence to refine fine-grained model decisions,” *IEEE Transactions on Pattern Analysis and Machine Intelligence*, vol. 43, no. 11, pp. 4196–4202, 2021.
- [4] K. Simonyan, A. Vedaldi, and A. Zisserman, “Deep inside convolutional networks: Visualising image classification models and saliency maps,” *arXiv preprint arXiv:1312.6034*, 2013.
- [5] R. R. Selvaraju, M. Cogswell, A. Das, R. Vedantam, D. Parikh, and D. Batra, “Grad-cam: Visual explanations from deep networks via gradient-based localization,” in *Proceedings of the IEEE international conference on computer vision*, 2017, pp. 618–626.
- [6] J. T. Springenberg, A. Dosovitskiy, T. Brox, and M. Riedmiller, “Striving for simplicity: The all convolutional net,” 2014.
- [7] A. Shrikumar, P. Greenside, and A. Kundaje, “Learning important features through propagating activation differences,” in *Proceedings of the 34th International Conference on Machine Learning*, ser. Proceedings of Machine Learning Research, D. Precup and Y. W. Teh, Eds., vol. 70. PMLR, 06–11 Aug 2017, pp. 3145–3153.
- [8] A.-K. Dombrowski, M. Alber, C. J. Anders, M. Ackermann, K.-R. Müller, and P. Kessel, “Explanations can be manipulated and geometry is to blame,” 2019.

- [9] M. Sundararajan, A. Taly, and Q. Yan, "Axiomatic attribution for deep networks," in *International conference on machine learning*. PMLR, 2017, pp. 3319–3328.
- [10] P. Lipton, "Contrastive explanation," *Royal Institute of Philosophy Supplement*, vol. 27, p. 247–266, 1990.
- [11] S. Wachter, B. Mittelstadt, and C. Russell, "Counterfactual explanations without opening the black box: Automated decisions and the gdpr," 2017.
- [12] S. M. Lundberg and S.-I. Lee, "A unified approach to interpreting model predictions," *Advances in neural information processing systems*, vol. 30, 2017.
- [13] P. Wang and N. Vasconcelos, "Scout: Self-aware discriminant counterfactual explanations," in *Proceedings of the IEEE/CVF Conference on Computer Vision and Pattern Recognition (CVPR)*, June 2020.
- [14] R. Chen, H. Zhang, S. Liang, J. Li, and X. Cao, "Less is more: Fewer interpretable region via submodular subset selection," in *International Conference on Learning Representations*, 2024.
- [15] A. Dhurandhar, P. Chen, R. Luss, C. Tu, P. Ting, K. Shanmugam, and P. Das, "Explanations based on the missing: Towards contrastive explanations with pertinent negatives," *CoRR*, vol. abs/1802.07623, 2018.
- [16] R. Chen, J. Li, H. Zhang, C. Sheng, L. Liu, and X. Cao, "Sim2word: Explaining similarity with representative attribute words via counterfactual explanations," *ACM Trans. Multimedia Comput. Commun. Appl.*, vol. 19, no. 6, jul 2023.
- [17] M. Sundararajan and A. Najmi, "The many shapley values for model explanation," in *International conference on machine learning*. PMLR, 2020, pp. 9269–9278.
- [18] V. Miglani, N. Kokhlikyan, B. Alsallakh, M. Martin, and O. Reblitz-Richardson, "Investigating saturation effects in integrated gradients," *CoRR*, vol. abs/2010.12697, 2020.
- [19] G. Erion, J. D. Janizek, P. Sturmfels, S. M. Lundberg, and S.-I. Lee, "Improving performance of deep learning models with axiomatic attribution priors and expected gradients," *Nature machine intelligence*, vol. 3, no. 7, pp. 620–631, 2021.
- [20] P. Sturmfels, S. Lundberg, and S.-I. Lee, "Visualizing the impact of feature attribution baselines," *Distill*, 2020, <https://distill.pub/2020/attribution-baselines>.
- [21] O. Russakovsky, J. Deng, H. Su, J. Krause, S. Satheesh, S. Ma, Z. Huang, A. Karpathy, A. Khosla, M. Bernstein, A. C. Berg, and L. Fei-Fei, "ImageNet Large Scale Visual Recognition Challenge," *International Journal of Computer Vision (IJCV)*, vol. 115, no. 3, pp. 211–252, 2015.
- [22] C. Szegedy, V. Vanhoucke, S. Ioffe, J. Shlens, and Z. Wojna, "Re-thinking the inception architecture for computer vision," *CoRR*, vol. abs/1512.00567, 2015.
- [23] A. Kapishnikov, S. Venugopalan, B. Avci, B. Wedin, M. Terry, and T. Bolukbasi, "Guided integrated gradients: An adaptive path method for removing noise," in *Proceedings of the IEEE/CVF Conference on Computer Vision and Pattern Recognition*, 2021, pp. 5050–5058.
- [24] S. Xu, S. Venugopalan, and M. Sundararajan, "Attribution in scale and space," in *2020 IEEE/CVF Conference on Computer Vision and Pattern Recognition (CVPR)*, 2020, pp. 9677–9686.
- [25] M.-J. Wu, J.-S. R. Jang, and J.-L. Chen, "Wafer map failure pattern recognition and similarity ranking for large-scale data sets," *IEEE Transactions on Semiconductor Manufacturing*, vol. 28, no. 1, pp. 1–12, 2015.
- [26] A. Kapishnikov, T. Bolukbasi, F. Viegas, and M. Terry, "Xrai: Better attributions through regions," in *2019 IEEE/CVF International Conference on Computer Vision (ICCV)*. Los Alamitos, CA, USA: IEEE Computer Society, nov 2019, pp. 4947–4956.
- [27] D. Smilkov, N. Thorat, B. Kim, F. B. Viégas, and M. Wattenberg, "Smoothgrad: removing noise by adding noise," *CoRR*, vol. abs/1706.03825, 2017.
- [28] S. Verma, J. Dickerson, and K. Hines, "Counterfactual explanations for machine learning: A review," *arXiv preprint arXiv:2010.10596*, 2020.
- [29] A. Madry, A. Makelov, L. Schmidt, D. Tsipras, and A. Vladu, "Towards deep learning models resistant to adversarial attacks," in *International Conference on Learning Representations*, 2018.
- [30] A. Ignatiev, N. Narodytska, and J. Marques-Silva, "On relating explanations and adversarial examples," *Advances in neural information processing systems*, vol. 32, 2019.
- [31] E. J. Friedman, "Paths and consistency in additive cost sharing," *International Journal of Game Theory*, vol. 32, no. 4, pp. 501–518, 2004.
- [32] K. Abhishek and D. Kamath, "Attribution-based xai methods in computer vision: A review," *arXiv preprint arXiv:2211.14736*, 2022.
- [33] M. D. Zeiler and R. Fergus, "Visualizing and understanding convolutional networks," in *European conference on computer vision*. Springer, 2014, pp. 818–833.
- [34] B. Zhou, A. Khosla, A. Lapedriza, A. Oliva, and A. Torralba, "Learning deep features for discriminative localization," in *Proceedings of the IEEE conference on computer vision and pattern recognition*, 2016, pp. 2921–2929.
- [35] M. T. Ribeiro, S. Singh, and C. Guestrin, "Why should i trust you?" explaining the predictions of any classifier," in *Proceedings of the 22nd ACM SIGKDD international conference on knowledge discovery and data mining*, 2016, pp. 1135–1144.
- [36] "A value for n-person games," *Classics in game theory*, vol. 69.
- [37] Y. Matsui and T. Matsui, "Np-completeness for calculating power indices of weighted majority games," *Theoretical Computer Science*, vol. 263, no. 1-2, pp. 305–310, 2001.
- [38] E. Strumbelj and I. Kononenko, "An efficient explanation of individual classifications using game theory," *The Journal of Machine Learning Research*, vol. 11, pp. 1–18, 2010.
- [39] R. Mitchell, J. Cooper, E. Frank, and G. Holmes, "Sampling permutations for shapley value estimation," 2022.
- [40] J. Chen, L. Song, M. J. Wainwright, and M. I. Jordan, "L-shapley and c-shapley: Efficient model interpretation for structured data," *arXiv preprint arXiv:1808.02610*, 2018.
- [41] G. Wang, Y.-N. Chuang, M. Du, F. Yang, Q. Zhou, P. Tripathi, X. Cai, and X. Hu, "Accelerating shapley explanation via contributive cooperators selection," in *International Conference on Machine Learning*. PMLR, 2022, pp. 22576–22590.
- [42] M. Ancona, C. Oztireli, and M. Gross, "Explaining deep neural networks with a polynomial time algorithm for shapley value approximation," in *International Conference on Machine Learning*. PMLR, 2019, pp. 272–281.
- [43] N. Jethani, M. Sudarshan, I. C. Covert, S.-I. Lee, and R. Ranganath, "Fastshap: Real-time shapley value estimation," in *International Conference on Learning Representations*, 2021.
- [44] M. Ancona, E. Ceolini, C. Oztireli, and M. Gross, "Towards better understanding of gradient-based attribution methods for deep neural networks," *arXiv preprint arXiv:1711.06104*, 2017.
- [45] N. Akhtar, M. Jalwana, M. Bennamoun, and A. S. Mian, "Attack to fool and explain deep networks," *IEEE Transactions on Pattern Analysis and Machine Intelligence*, pp. 1–1, 2021.
- [46] Y. Dong, F. Bao, H. Su, and J. Zhu, "Towards interpretable deep neural networks by leveraging adversarial examples," *CoRR*, vol. abs/1901.09035, 2019.
- [47] M. Zhu, T. Chen, and Z. Wang, "Sparse and imperceptible adversarial attack via a homotopy algorithm," 2021.
- [48] A. Ilyas, S. Santurkar, D. Tsipras, L. Engstrom, B. Tran, and A. Madry, "Adversarial examples are not bugs, they are features," *Advances in neural information processing systems*, vol. 32, 2019.
- [49] C.-H. Lee, Z. Liu, L. Wu, and P. Luo, "Maskgan: Towards diverse and interactive facial image manipulation," in *IEEE Conference on Computer Vision and Pattern Recognition (CVPR)*, 2020.
- [50] Y. Liu, S. Khandagale, C. White, and W. Neiswanger, "Synthetic benchmarks for scientific research in explainable machine learning," *CoRR*, vol. abs/2106.12543, 2021.
- [51] Z. Bylinskii, T. Judd, A. Oliva, A. Torralba, and F. Durand, "What do different evaluation metrics tell us about saliency models?" *IEEE Transactions on Pattern Analysis and Machine Intelligence*, vol. 41, no. 3, pp. 740–757, 2019.
- [52] X. Li and D. Roth, "Learning question classifiers," in *The 19th International Conference on Computational Linguistics*, 2002.
- [53] Y. Kim, "Convolutional neural networks for sentence classification," *CoRR*, vol. abs/1408.5882, 2014.
- [54] Z. Liu, P. Luo, X. Wang, and X. Tang, "Deep learning face attributes in the wild," in *Proceedings of International Conference on Computer Vision (ICCV)*, December 2015.
- [55] M. Sandler, A. G. Howard, M. Zhu, A. Zhmoginov, and L. Chen, "Inverted residuals and linear bottlenecks: Mobile networks for classification, detection and segmentation," *CoRR*, vol. abs/1801.04381, 2018.
- [56] T. Salimans, I. J. Goodfellow, W. Zaremba, V. Cheung, A. Radford, and X. Chen, "Improved techniques for training gans," *CoRR*, vol. abs/1606.03498, 2016.

APPENDIX A

IMPLEMENTATION DETAILS

A.1 Step size and number

Fig. A.1a shows the objective loss (Eq. 4 in main paper) curves during the optimization for GradPath, and Fig. A.1b shows IG^2 attributions w.r.t. different step sizes and numbers.

We choose a moderate step size that can deal well with the trade-off between attribution noise and completeness. The specific hyper-parameters about step size and number for different datasets are reported in Table A.1.

A.2 Normalization

We consider two normalization methods: ℓ_2 norm and ℓ_1 norm. Given the gradient $g_\alpha = \frac{\partial \|\hat{f}(\gamma^G(\alpha)) - f(\alpha)\|_2}{\partial \gamma^G(\alpha)}$ at step α , we can have $W_\alpha^{\ell_2}$ and $W_\alpha^{\ell_1}$:

ℓ_2 norm is simple:

$$W_\alpha^{\ell_2} = \|g_\alpha\|_2, \quad (20)$$

which is used in previous works about adversarial robustness [29], [48].

ℓ_1 norm is more tricky. Following a sparse adversarial attack work [47], an additional parameter k that controls the sparsity of gradient on each step is introduced. Specifically, we select the features i with top k maximal absolute gradient value and then normalize the sparse vector with sign function:

$$W_\alpha^{\ell_1}(i) = \begin{cases} |S|g(i), & i \in S = \underset{|A|=k}{\operatorname{argmax}} \sum_{i \in A} |g(i)| \\ 0 & \end{cases}, \quad (21)$$

where S is the set contains the index of top k maximal absolute value in vector g and the set size $|S|$ is the ℓ_1 norm of signed vector.

Both ℓ_1 and ℓ_2 normalization imply the feature importance on each step perturbation, the comparison of which is presented below. In practice, we use more general ℓ_2 normalization by default.

We compare ℓ_2 and ℓ_1 normalization for the gradient of GradPath (i.e., W). ℓ_1 normalization has an additional parameter to control sparsity, which is presented by the percentile of the gradient vector. Fig. A.2 plots the IG^2 attributions on wafer map under different normalizations. When the percentile is low (90), the attribution under ℓ_1 normalization resembles ℓ_2 . When the attribution sparsity increases, the noises significantly drop, but some attributions on relevant features also get very small, which especially damages the performance of certain classes (e.g., Donut, Near-full, and Random). This can be regarded as a precision and recall trade-off.

TABLE A.1: IG^2 hyper-parameters for different datasets

Datasets	Input region	Step size	Steps	Ref.
ImageNet	[0,255]	1024	500	random (trick)
TREC	[-1.156, 1.094]	0.01	1000	random
wafer map	[0,1]	0.02	2000	the normal

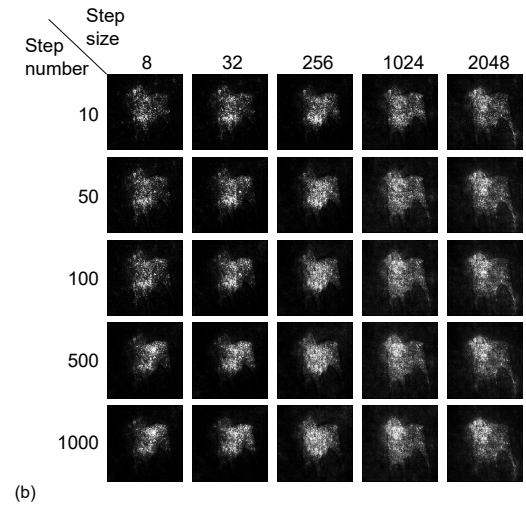
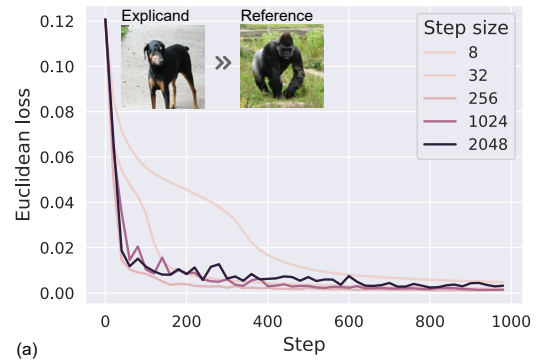


Fig. A.1: (a) Curves of loss w.r.t. step numbers for different step sizes. (b) IG^2 attributions w.r.t. step sizes and numbers. [Doberman] is explained with reference [gorilla].

A.3 Representation layer

We compare the IG^2 with the different representation layers of wafer map classifier (Table B.5), which is shown in Fig. A.3. GradCFE gets less noise using the deeper layer as representation, while IG^2 is slightly affected by the choice of representation layer.

A.4 Representation distance measure

We compare the representation distance measures of IG^2 . Fig. A.4 shows the ImageNet sample attributions by three measures, as an intuitive illustration of main paper Table A.2. Generally, IG^2 with Euclidean distance and Cosine similarity provide very similar feature attributions, while ℓ_1 norm will introduce unpleasant noises.

A.5 Computational cost

Table A.3 reports the average computation time per explained sample. For a fair comparison, all the methods run with the same step number and batch size (if available). We run the experiments with 1 NVIDIA GeForce GTX 1080 Ti GPU. The KernelSHAP applies the superpixel technique for ImageNet and wafer map datasets.

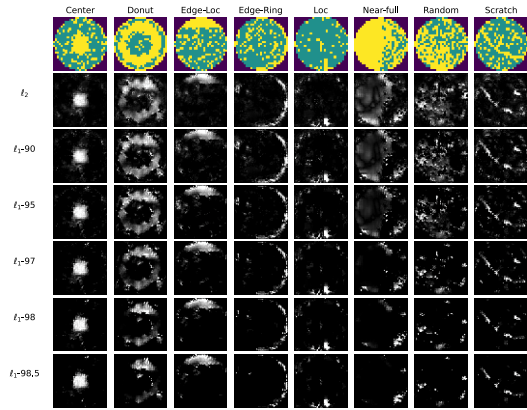


Fig. A.2: IG^2 attributions of ℓ_1 and ℓ_2 normalization. Five sparsity percentile parameters (90, 95, 97, 98, 98.5) of ℓ_1 normalization are compared.

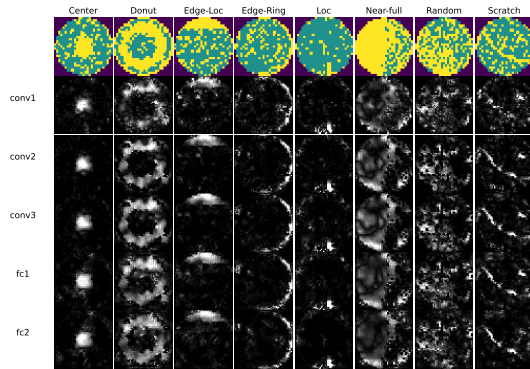


Fig. A.3: IG^2 with the different representation layer (fc1 used in the paper).

TABLE A.2: Evaluation of model representation distance measures (the gap to Euclidean distance)

Datasets	Measures	Ground truth		SIC AUC	
		AUC \uparrow	SUM \uparrow	ADD \uparrow	DEL \downarrow
ImageNet	Cosine	-0.055	-0.021	+0.018	+0.047
	ℓ_1 norm	-0.065	-0.027	-0.028	+0.003
TREC	Cosine	—		+0.009	+0.007
	ℓ_1 norm	—		-0.010	+0.012
Wafer map	Cosine	-0.024	-0.019	-0.010	-0.002
	ℓ_1 norm	-0.072	-0.037	-0.029	+0.016

APPENDIX B DATASETS AND EXPLAINED MODELS

B.1 MNIST classification

Fig. A.5 validates the most critical areas in digital 5 that distinguishes the explicand to references of digitals 3, 6, 9. We compare the areas highlighted by IG^2 (the areas in the

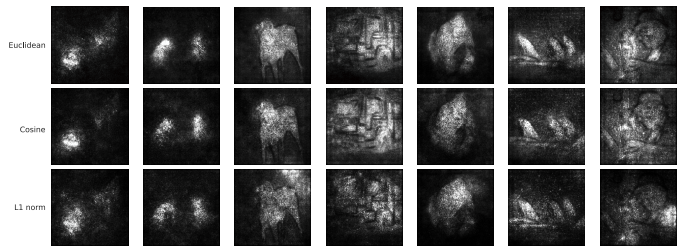


Fig. A.4: IG^2 attributions of Euclidean, Cosine, and ℓ_1 norm measures (Euclidean distance used in the paper). TABLE A.3: Average explanation time per sample (sec.). The input feature numbers of KernelSHAP are reduced.

	ImageNet	TREC	wafermap
Gradient	0.13	0.003	0.03
Vanilla IG	8.14	0.26	0.89
Guided IG	37.0	4.48	6.39
Expected IG	8.34	0.49	1.25
DeepSHAP	111.0	0.32	0.95
KernelSHAP	3150.2 (13 \times 13)	1.8	75.0 (28 \times 28)
IG^2	108.2	9.80	18.3

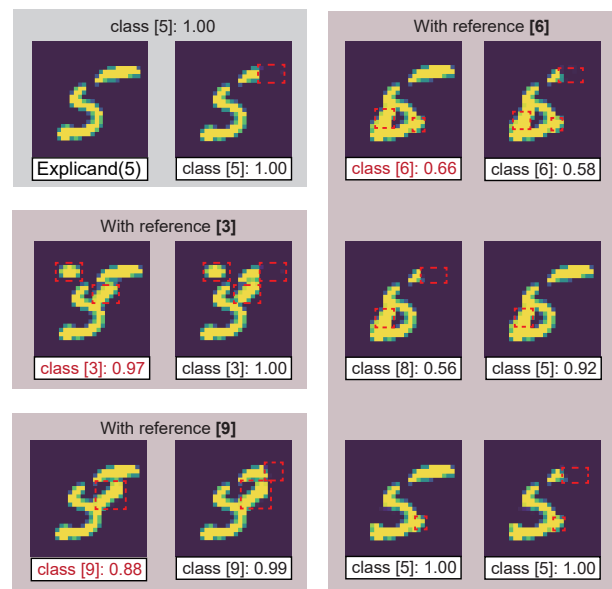


Fig. A.5: Ablation study for critical areas in the explained digital 5 with references of digitals 3, 6, 9. The titles of each subfigure report the predicted class with Softmax output. The areas in the first figure of each block (with red titles) are used in main paper Fig. 6.

figures with red titles) and the areas of Expected IG (the right upper corners). We study the importance of different areas by the permutations: We first remove the right upper pixels of digital 5, which does not change model prediction. If we fill the highlighted areas of IG^2 with pixels, the model predicts the modified digitals as the class labels of references. Based on this, if we further remove the right upper corners of these digitals, the impact on model predictions is not significant.

In sum, compared with the right upper corners of Ex-

TABLE A.4: The structure of MLP to be explained for the regression on the synthetic dataset from XAI-BENCH

Layer	Configuration
input	5-Dimension vector
fc1	fc _{5,64} +BN+Tanh
fc2	conv _{64,16} +Tanh
fc3	conv _{16,1}

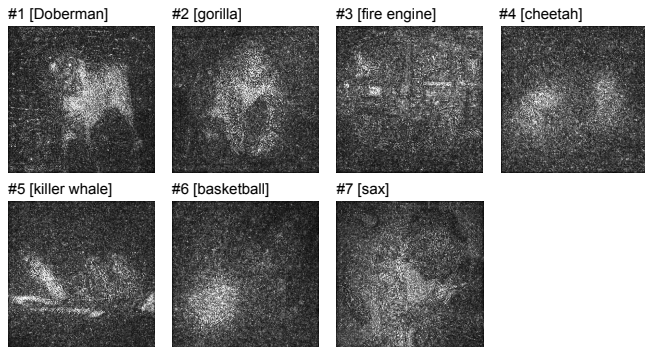


Fig. B.6: GradCFE for the ImageNet images in main paper Fig. 7, showing the general counterfactual directions of GradPath (from the explicand to its GradCF).

pected IG, the areas highlighted by IG² are more critical for distinguishing the explicand to references. Besides, we believe areas of IG² are also closer to the intuition.

B.2 Synthetic dataset in XAI-BENCH

We synthesize the dataset x from the 5-dimension Gaussian distribution with $\mu = \vec{0}$ and $\Sigma = I_5$. The additive piecewise function for labels are [50]:

$$\begin{aligned} \psi_1(x_1) &= 1 \text{ if } x_1 \geq 0, \text{ otherwise } -1, \\ \psi_2(x_2) &= \begin{cases} -2 & , x_2 < -0.5 \\ -1 & , -0.5 \leq x_2 < 0 \\ 1 & , 0 \leq x_2 < 0.5 \\ 2 & , x_2 \geq 0.5 \end{cases}, \\ \psi_3(x_3) &= \lfloor 2\cos(\pi x_3) \rfloor, \\ \psi_i(x_i) &= 0, \quad i = 4, 5, \end{aligned} \quad (22)$$

and we cut off the normalized function output with a threshold to obtain the binary label:

$$y = \begin{cases} 1 & , \text{ if } \text{Norm}[\sum_{i=1}^5 \psi_i] > 0 \\ 0 & , \text{ if } \text{Norm}[\sum_{i=1}^5 \psi_i] \leq 0 \end{cases}, \quad (23)$$

where $\text{Norm}[\]$ makes the mean value of outputs zero.

The structure Multi-Layer Perceptron (MLP) trained on the synthetic dataset is reported in Table A.4.

B.3 ImageNet classification

Fig. B.6 shows the GradCFE for the explicand displayed in main paper Fig. 7. GradCFE presents the difference between the explicand and its baseline, GradCF. Fig. B.6 illustrates that the integration path of IG² is in the direction of critical features, which can mitigate the saturation effects.

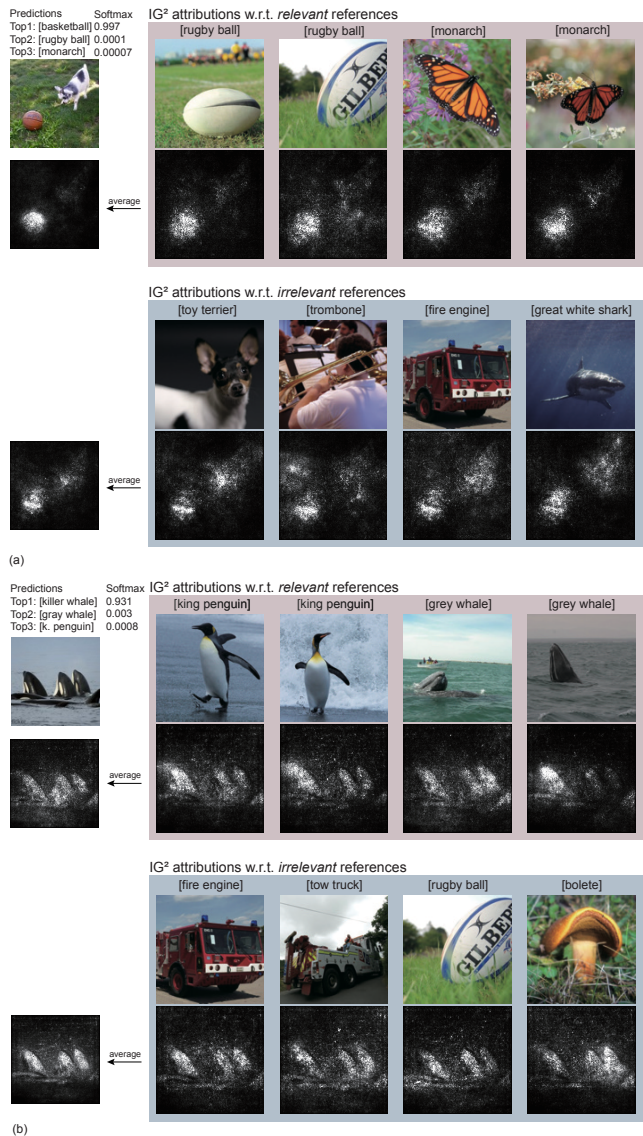


Fig. B.7: Feature attributions with regard to different references, as a supplement for main paper Fig. 11. (a) Explained image of class [basketball] with interference object “dog”. (b) Explained image of class [killer whale] on pure background.

As a supplement for main paper Fig. 11, Fig. B.7 shows the feature attributions with regard to different categories of references for two more ImageNet samples. This supports the analyses of reference impact and choice trick.

B.4 TREC classification

Fig. B.8 shows the complete word attribution results of all compared methods. The results are consistent with the conclusions made in the main paper that IG² makes less attributions on weak interrogative words and more attributions on critical phrases.

B.5 Wafermap failure pattern classification

Fig. B.9 plots the wafer maps sampled from WM-811K dataset [25], including three images per class. To achieve the

[Predictions]	[Questions with explanations]
#1 [LOCATION]	<p>[IG²] What are the only two states that incorporate the Confederate battle flag in their flags ?</p> <p>[Gradient] What are the only two states that incorporate the Confederate battle flag in their flags ?</p> <p>[IG] What are the only two states that incorporate the Confederate battle flag in their flags ?</p> <p>[Guided IG] What are the only two states that incorporate the Confederate battle flag in their flags ?</p> <p>[Expected IG] What are the only two states that incorporate the Confederate battle flag in their flags ?</p> <p>[DeepSHAP] What are the only two states that incorporate the Confederate battle flag in their flags ?</p> <p>[KernelSHAP] What are the only two states that incorporate the Confederate battle flag in their flags ?</p>
#2 [LOCATION]	<p>[IG²] Where did guinea pigs originate ?</p> <p>[Gradient] Where did guinea pigs originate ?</p> <p>[IG] Where did guinea pigs originate ?</p> <p>[Guided IG] Where did guinea pigs originate ?</p> <p>[Expected IG] Where did guinea pigs originate ?</p> <p>[DeepSHAP] Where did guinea pigs originate ?</p> <p>[KernelSHAP] Where did guinea pigs originate ?</p>
#3 [ENTITY]	<p>[IG²] Which drug is commonly used to treat AIDS ?</p> <p>[Gradient] Which drug is commonly used to treat AIDS ?</p> <p>[IG] Which drug is commonly used to treat AIDS ?</p> <p>[Guided IG] Which drug is commonly used to treat AIDS ?</p> <p>[Expected IG] Which drug is commonly used to treat AIDS ?</p> <p>[DeepSHAP] Which drug is commonly used to treat AIDS ?</p> <p>[KernelSHAP] Which drug is commonly used to treat AIDS ?</p>
#4 [ENTITY]	<p>[IG²] What was the name of the Protestant revolt against the supremacy of the Pope ?</p> <p>[Gradient] What was the name of the Protestant revolt against the supremacy of the Pope ?</p> <p>[IG] What was the name of the Protestant revolt against the supremacy of the Pope ?</p> <p>[Guided IG] What was the name of the Protestant revolt against the supremacy of the Pope ?</p> <p>[Expected IG] What was the name of the Protestant revolt against the supremacy of the Pope ?</p> <p>[DeepSHAP] What was the name of the Protestant revolt against the supremacy of the Pope ?</p> <p>[KernelSHAP] What was the name of the Protestant revolt against the supremacy of the Pope ?</p>
#5 [DESCRIPTION]	<p>[IG²] What is the difference between microprocessors & microcontrollers ?</p> <p>[Gradient] What is the difference between microprocessors & microcontrollers ?</p> <p>[IG] What is the difference between microprocessors & microcontrollers ?</p> <p>[Guided IG] What is the difference between microprocessors & microcontrollers ?</p> <p>[Expected IG] What is the difference between microprocessors & microcontrollers ?</p> <p>[DeepSHAP] What is the difference between microprocessors & microcontrollers ?</p> <p>[KernelSHAP] What is the difference between microprocessors & microcontrollers ?</p>
#6 [DESCRIPTION]	<p>[IG²] How do you make panoramic sugar eggs for Easter - the ones with the scene inside ?</p> <p>[Gradient] How do you make panoramic sugar eggs for Easter - the ones with the scene inside ?</p> <p>[IG] How do you make panoramic sugar eggs for Easter - the ones with the scene inside ?</p> <p>[Guided IG] How do you make panoramic sugar eggs for Easter - the ones with the scene inside ?</p> <p>[Expected IG] How do you make panoramic sugar eggs for Easter - the ones with the scene inside ?</p> <p>[DeepSHAP] How do you make panoramic sugar eggs for Easter - the ones with the scene inside ?</p> <p>[KernelSHAP] How do you make panoramic sugar eggs for Easter - the ones with the scene inside ?</p>
#7 [HUMAN]	<p>[IG²] Who sought to create The Great Society ?</p> <p>[Gradient] Who sought to create The Great Society ?</p> <p>[IG] Who sought to create The Great Society ?</p> <p>[Guided IG] Who sought to create The Great Society ?</p> <p>[Expected IG] Who sought to create The Great Society ?</p> <p>[DeepSHAP] Who sought to create The Great Society ?</p> <p>[KernelSHAP] Who sought to create The Great Society ?</p>
#8 [HUMAN]	<p>[IG²] What are the characters' names in the Scooby-Doo cartoon ?</p> <p>[Gradient] What are the characters' names in the Scooby-Doo cartoon ?</p> <p>[IG] What are the characters' names in the Scooby-Doo cartoon ?</p> <p>[Guided IG] What are the characters' names in the Scooby-Doo cartoon ?</p> <p>[Expected IG] What are the characters' names in the Scooby-Doo cartoon ?</p> <p>[DeepSHAP] What are the characters' names in the Scooby-Doo cartoon ?</p> <p>[KernelSHAP] What are the characters' names in the Scooby-Doo cartoon ?</p>
#9 [NUMERIC]	<p>[IG²] What are the lengths of pearl necklaces ?</p> <p>[Gradient] What are the lengths of pearl necklaces ?</p> <p>[IG] What are the lengths of pearl necklaces ?</p> <p>[Guided IG] What are the lengths of pearl necklaces ?</p> <p>[Expected IG] What are the lengths of pearl necklaces ?</p> <p>[DeepSHAP] What are the lengths of pearl necklaces ?</p> <p>[KernelSHAP] What are the lengths of pearl necklaces ?</p>
#10 [NUMERIC]	<p>[IG²] How long does it take the typical hen to lay 19 dozen eggs ?</p> <p>[Gradient] How long does it take the typical hen to lay 19 dozen eggs ?</p> <p>[IG] How long does it take the typical hen to lay 19 dozen eggs ?</p> <p>[Guided IG] How long does it take the typical hen to lay 19 dozen eggs ?</p> <p>[Expected IG] How long does it take the typical hen to lay 19 dozen eggs ?</p> <p>[DeepSHAP] How long does it take the typical hen to lay 19 dozen eggs ?</p> <p>[KernelSHAP] How long does it take the typical hen to lay 19 dozen eggs ?</p>

Fig. B.8: Word attributions of all compared methods for TREC dataset, as a complement for main paper Fig. 8.

task of failure pattern classification, we select a small subset of WM-811K dataset with a total of 19000 wafer maps. The backbone of the classification neural network is based on convolution, the detailed structure of which is reported in Table B.5.

B.6 CelebA face attribute classification

Face attribute classification in CelebA is a multi-label task. There are totally 40 face attributes with binary labels. The classification accuracy for each face attributes are reported in Table B.6.

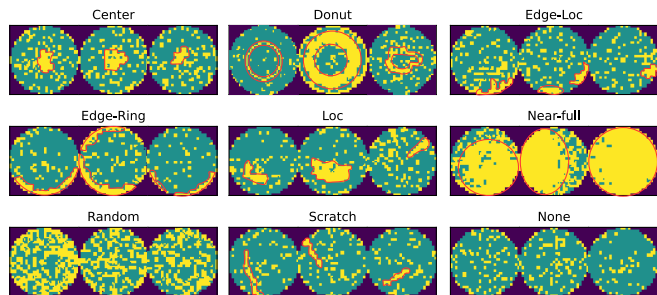


Fig. B.9: The sampled wafer map images from WM-811K dataset, including eight failure patterns and one without any pattern: [Center], [Donut], [Edge-Loc], [Edge-Ring], [Loc], [Near-full], [Random], [Scratch] and [None]. The failure cause position (pixels) are also annotated in the red border area (except [Random] and [None]).

TABLE B.5: The structure of CNN to be explained for wafer map failure pattern classification

Layer	Configuration
input	$56 \times 56 \times 3$ RGB images
conv1	conv _{3,32,3} +ReLU+Pool
conv2	conv _{32,64,3} +ReLU+Pool
conv3	conv _{64,128,3} +ReLU+Pool
fc1	fc _{8192,1250} +ReLU
fc2	fc _{1250,9} +Softmax

TABLE B.6: Classification accuracy on each face attribute of CelebA

Attributes	Acc. (%)	Attributes	Acc. (%)
5_o_Clock_Shadow	94.4	Male	97.9
Arched_Eyebrows	83.4	Mouth_Slightly_Open	93.6
Attractive	82.5	Mustache	96.9
Bags_Under_Eyes	85.0	Narrow_Eyes	87.7
Bald	98.9	No_Beard	96.0
Bangs	95.9	Oval_Face	75.4
Big_Lips	71.3	Pale_Skin	97.0
Big_Nose	84.6	Pointy_Nose	77.1
Black_Hair	89.0	Receding_Hairline	93.7
Blond_Hair	95.6	Rosy_Cheeks	94.9
Blurry	95.9	Sideburns	97.7
Brown_Hair	88.2	Smiling	92.7
Bushy_Eyebrows	92.6	Straight_Hair	83.4
Chubby	95.3	Wavy_Hair	83.4
Double_Chin	96.2	Wearing_Earrings	90.4
Eyeglasses	99.6	Wearing_Hat	99.0
Goatee	97.5	Wearing_Lipstick	93.7
Gray_Hair	98.3	Wearing_Necklace	87.5
Heavy_Makeup	91.3	Wearing_Necktie	96.7
High_Cheekbones	86.8	Young	88.2
		Average	91.0

For the ground truth in quantitative evaluation of celebA attribution (in main paper Table 3), we utilize the face parsing model pretrained on CelebAMask-HQ [49] to split the face image into different facial components, such as hair,

nose and eyes. The ground truth is chosen as the facial components that are most related to the explained face attribute. Table B.7 gives the correspondences between explained face attributes (of CelebA) and parsed facial components (of CelebAMask-HQ). In quantitative evaluation, we only consider the face attributes that have explicit corresponding components.

TABLE B.7: Correspondences between explained face attributes and parsed facial components

Attributes	Comp.	Attributes	Comp.
5_o_Clock_Shadow	-	Male	-
Arched_Eyebrows	brows	Mouth_Slightly_Open	mouth
Attractive	-	Mustache	-
Bags_Under_Eyes	eyes	Narrow_Eyes	eyes
Bald	hair	No_Beard	-
Bangs	hair	Oval_Face	-
Big_Lips	lips	Pale_Skin	skin
Big_Nose	nose	Pointy_Nose	nose
Black_Hair	hair	Receding_Hairline	hair
Blond_Hair	hair	Rosy_Cheeks	-
Blurry	-	Sideburns	hair
Brown_Hair	hair	Smiling	mouth
Bushy_Eyebrows	brows	Straight_Hair	hair
Chubby	-	Wavy_Hair	hair
Double_Chin	-	Wearing_Earrings	ear_r
Eyeglasses	eye_g	Wearing_Hat	hat
Goatee	-	Wearing_Lipstick	lips
Gray_Hair	hair	Wearing_Necklace	neck_l
Heavy_Makeup	-	Wearing_Necktie	cloth
High_Cheekbones	-	Young	-